Calcium and magnesium ions modulate the oligomeric state and function of mitochondrial 2-Cys peroxiredoxins in *Leishmania* parasites

Received for publication, October 5, 2016, and in revised form, March 7, 2017 Published, Papers in Press, March 14, 2017, DOI 10.1074/jbc.M116.762039

Mariana A. B. Morais[‡1], Priscila O. Giuseppe[‡], Tatiana A. C. B. Souza[§], Helena Castro[¶‖2], Rodrigo V. Honorato[‡], Paulo S. L. Oliveira[‡], Luis E. S. Netto, Ana M. Tomas[¶‖‡‡], and Mario T. Murakami[‡3]**

*From the [‡]Biosciences National Laboratory, National Center for Research in Energy and Materials, Rua Giuseppe Maximo Scolfaro 10000, 13083-100 Campinas/SP, Brazil, the [§]Proteomics and Protein Engineering Laboratory, Carlos Chagas Institute, Fiocruz, Rua Professor Algacyr Munhoz Mader 2135, 81310-020 Curitiba/PR, Brazil, the [¶]i3S-Institute for Investigation and Innovation in Health, University of Porto, Rua Alfredo Allen 208, 4200-135 Porto, Portugal, the [‖]Institute of Molecular and Cell Biology (IBMC), University of Porto, Rua Alfredo Allen 208, 4200-135 Porto, Portugal, the **Department of Genetics and Evolutionary Biology, Institute of Biosciences, University of the State of São Paulo, Rua do Matão 14, 05508-090 São Paulo/SP, Brazil, and the [‡‡]Abel Salazar Biomedical Sciences Institute, University of Porto, Rua de Jorge Viterbo Ferreira 228, 4050-313 Porto, Portugal*

Edited by Thomas Söllner

Leishmania **parasites have evolved a number of strategies to cope with the harsh environmental changes during mammalian infection. One of these mechanisms involves the functional gain that allows mitochondrial 2-Cys peroxiredoxins to act as molecular chaperones when forming decamers. This function is critical for parasite infectivity in mammals, and its activation has been considered to be controlled exclusively by the enzyme redox state under physiological conditions. Herein, we have revealed that magnesium and calcium ions play a major role in modulating the ability of these enzymes to act as molecular chaperones, surpassing the redox effect. These ions are directly involved in mitochondrial metabolism and participate in a novel mechanism to stabilize the decameric form of 2-Cys peroxiredoxins in** ***Leishmania*** **mitochondria. Moreover, we have demonstrated that a constitutively dimeric Prx1m mutant impairs the survival of** ***Leishmania*** **under heat stress, supporting the central role of the chaperone function of Prx1m for** ***Leishmania*** **parasites during the transition from insect to mammalian hosts.**

The *Leishmania* parasites, causative agents of human and canine leishmaniasis, are exposed to different growth conditions during their life cycle because of the migration from the insect to the mammalian host environment. Among the differences are the elevation of temperature, exposure to oxidants produced by the macrophages, pH acidification, and lower availability of oxygen and nutrients (1). In this context, parasite survival as well as the establishment of a successful intracellular infection relies on the development of adaptive mechanisms for hostile conditions. In *Leishmania infantum*, for instance, one such mechanism involves mitochondrial 2-Cys peroxiredoxin (*Li*Prx1m)[4] (2), also named tryparedoxin peroxidase, which allows the parasite to cope with heat stress during the transition from the insect (25 °C) to the mammalian host (37 °C) (2, 3).

Prx1 subfamily members are peroxide-scavenging enzymes that display a 2-Cys catalytic mechanism and can assume distinct oligomeric states (dimers, decamers, and higher-order oligomers) (4). A dual function of peroxidase and molecular chaperone has been reported for several Prx1 enzymes and seems to be modulated by changes in quaternary structure (5–7). Factors such as the pH (8–10), ionic strength (8, 11, 12), protein concentration (3, 12, 13), and protein redox state (14, 15) can affect the dimer-decamer equilibrium of Prx1 members, but how these factors modulate the peroxidase and chaperone activities is still poorly understood. Overoxidation of peroxidasic cysteine, in particular, has been demonstrated to shut down the peroxidase function and to enhance the chaperone activity by stabilizing oligomers larger than decamers (5, 6). However, this functional switch appears to be relevant for only some members of Prx1 subfamily (16).

This work was supported by Grant 2010/51730-0 from the Fundação de Amparo à Pesquisa do Estado de São Paulo (FAPESP) and by grants from the Conselho Nacional de Desenvolvimento Científico e Tecnológico (CNPq) and the Coordenação de Aperfeiçoamento de Pessoal de Nível Superior (CAPES) (to M. T. M.). This work was also supported by grants from Project "NORTE-07-0124-FEDER-000002" (co-funded by the Norte Portugal Regional Operational Programme (NORTE 2020) under the Quadro de Referência Estratégico Nacional through the European Regional Development Fund (ERDF) and by the the Portuguese Foundation for Science and Technology) and from Project "NORTE-01-0145-FEDER-000012" (supported by NORTE 2020 under the PORTUGAL 2020 Partnership Agreement through ERDF) (to A. M. T.). The authors declare that they have no conflicts of interest with the contents of this article.

[1] Supported by FAPESP Fellowships 2011/10248-4, 2012/24134-3, and 2015/05851-4.

[2] Supported by the Portuguese Fundação para a Ciência e a Tecnologia (FCT) through the "Investigador FCT" programme.

[3] To whom correspondence should be addressed: Biosciences National Laboratory, National Center for Research in Energy and Materials, Giuseppe Maximo Scolfaro 10000, 13083-970 Campinas, São Paulo, Brazil. Tel.: 55-19-3512-1106; Fax: 55-19-3512-1100; E-mail: mario.murakami@lnbio.cnpem.br.

[4] The abbreviations used are: *Li*Prx1m, mitochondrial 2-Cys peroxiredoxin from *Leishmania infantum*; aSEC, analytical size-exclusion chromatography; C_p, peroxidatic cysteine; C_r, resolving cysteine; DLS, dynamic light scattering; DSF, differential scanning fluorimetry; *Hs*Prx2, human Prx2; *Lb*Prx1m, mitochondrial 2-Cys peroxiredoxin from *Leishmania braziliensis*; *Li*Prx1a, cytoplasmic 2-Cys peroxiredoxin from *Leishmania infantum*; PDB, Protein Data Bank; Prx, peroxiredoxin; SAXS, small angle X-ray scattering; SEC, size-exclusion chromatography; TEV, tobacco etch virus; TcPrx1a, cytoplasmic 2-Cys peroxiredoxin from *Trypanosoma cruzi*.

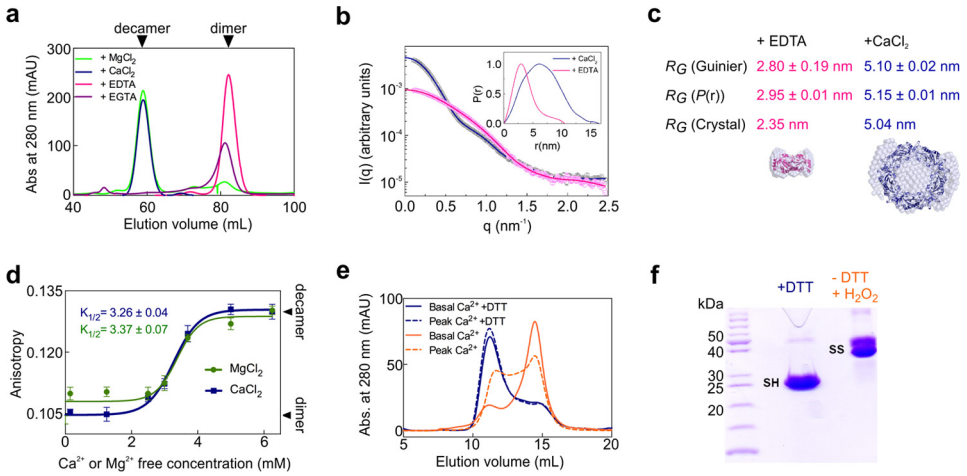

Figure 1. Ca^{2+} and Mg^{2+} ions induce the decamerization of *Lb*Prx1m. *a*, aSEC chromatograms of oxidized *Lb*Prx1m at 130 μM (2 ml) in a HiLoad Superdex 200 16/600 column pre-equilibrated with Tris buffer (pH 7.5) containing 25 mM $CaCl_2$, 25 mM $MgCl_2$, 5 mM EDTA, or 5 mM EGTA. *mAU*, milliabsorbance units. *b*, experimental SAXS curves (*open circles* with *error bars*) and theoretical scattering profiles (*lines*) computed from the *P*(r) function (*inset*) of oxidized *Lb*Prx1m (108 μM) in Tris buffer (pH 7.5) containing 25 mM $CaCl_2$ (*blue*) or 5 mM EDTA (*pink*). *c*, radius of gyration (R_G) for *Lb*Prx1m incubated with EDTA or $CaCl_2$, calculated independently from SAXS curves (*graph* in *b*), *P*(r) function (*inset* in *b*), or crystallographic data. The R_G value (*crystal*) was calculated from the scattering profiles computed for the crystal structures (PDB accession no. 4KB3 and 4KCE) using CRYSOL. The crystal structures of the dimer (*pink*) and the decamer (*blue*) are fitted into the respective envelopes calculated from SAXS data. *d*, fluorescence anisotropy data of oxidized *Lb*Prx1m preincubated at 80 μM with increasing concentrations of $MgCl_2$ or $CaCl_2$. The *lines* represent the nonlinear data fitting (Boltzmann sigmoid function) used to estimate $K_{1/2}$, *i.e.* the Mg^{2+} or Ca^{2+} concentration at which 50% of the dimers are converted to decamers. All measurements were performed in triplicate. *e*, aSEC chromatograms of *Lb*Prx1m at 100 μM (200 μl) in Tris buffer (pH 7.5) containing 700 μM $MgCl_2$ and 200 nM $CaCl_2$ (*solid lines*) or 90 μM $CaCl_2$ (*dashed lines*). The protein was incubated with 2 mM DTT (*blue lines*) or submitted to DTT treatment followed by DTT removal and protein oxidation using 100 μM H_2O_2 (*orange lines*). *f*, nonreducing SDS-PAGE confirming the reduced state (SH monomers) of DTT-treated samples and the oxidized state (S–S dimers) of samples pretreated with DTT and then oxidized with H_2O_2.

In *Leishmania*, the mitochondrial Prx1 can act as molecular chaperone and as a peroxidase, but only its role as chaperone is crucial for parasite infectivity in mammals (2, 3). Nonetheless, *in vitro* studies show that the peroxidase catalytic cycle modulates the chaperone reservoir of *Li*Prx1m, favoring chaperone-active decamers when reactive cysteine is reduced (C_p–SH) and chaperone-inactive dimers when C_p is oxidized into C_pS–SC_r (3). On the other hand, the enzyme from *Leishmania* mitochondrion (2) seems to be resistant to the over-oxidation mechanism that inactivates the peroxidase function, stabilizes high-order oligomers, and enhances the chaperone activity of fungal (5) and mammalian (6) 2-Cys Prx.

Recently, we have demonstrated that pH variations also affect the dimer-decamer equilibrium of *Leishmania braziliensis* Prx1m (*Lb*Prx1m), a close orthologue of the *L. infantum* enzyme, indicating that the chaperone function of these proteins might not be exclusively modulated by their redox state (9). A pH shift from 8.0 to 7.0, commonly observed in the mitochondria of nutrient-deprived cells (17), is sufficient to stabilize oxidized decamers of *Lb*Prx1m (9). Furthermore, it is unclear whether other factors from the mitochondrial environment affect the dimer-decamer interconversion of *Leishmania* Prx1m and its dual function. For 2-Cys Prx from distantly related species, it has been demonstrated that, at least *in vitro*, such equilibrium can be affected by ionic strength variations (11, 18) and post-translational modifications (19, 20).

Herein, we have demonstrated that the divalent cations Ca^{2+} and Mg^{2+}, which are important co-factors of mitochondrial enzymes involved in cellular respiration (21–23), activate the chaperone function of oxidized *Lb*Prx1m and enhance that of the reduced enzyme via a novel mechanism of decamer stabilization. Using an *Lb*Prx1m mutant unable to decamerize, we showed that decamer formation is crucial for both the chaperone and peroxidase activities of *Lb*Prx1m as well as for the protective role of this protein against heat stress in the parasite context. Together, our findings unveil an exclusive and redundant system in *Leishmania* that uses Ca^{2+} and Mg^{2+}, in addition to pH and redox mechanisms, to maintain most of Prx1m in the decameric form and hence support parasite survival and infectivity in the mammalian host.

Results

Ca^{2+}/Mg^{2+} ions induce LbPrx1m decamerization

Analytical size-exclusion chromatography (aSEC) and small-angle X-ray scattering (SAXS) experiments at physiological pH revealed that oxidized (disulfide-bonded) *Lb*Prx1m assumes a dimeric structure in the presence of chelating agents, whereas it assembles into decamers upon the addition of Ca^{2+} or Mg^{2+} (Fig. 1, *a*–*c*). Post-treatment of Ca^{2+} decamers with EDTA induced their disassembly into dimers, showing that the cation effect is a reversible process (Table 1). Upon comparison of several divalent cations, only Mg^{2+} and Ca^{2+} showed similar effects on *Lb*Prx1m oligomerization (Table 2), indicating a specific role for these ions in stabilizing *Lb*Prx1m decamers. The hypothesis that the Ca^{2+}/Mg^{2+} effect would be due to ionic strength variations in the medium was discarded, as *Lb*Prx1m presented the same SEC elution profile in the presence or absence of 150 mM NaCl (data not shown). As the effects of Mg^{2+} and Ca^{2+} were indistinguishable from each other, and because *Lb*Prx1m eluted as dimers when incubated with EGTA (Fig. 1*a*), which chelates Ca^{2+} with a higher selectivity ($>10^5$) (24) than Mg^{2+}, some of the *in vitro* and *in silico* assays described here were performed with Ca^{2+} only.

Table 1

DLS analysis of *Lb*Prx1m in the presence of $CaCl_2$

Samples were pretreated with $CaCl_2$ (I) and then incubated for 10 min with EDTA (II) to illustrate the reversibility of the decamerization process. Note that the hydrodynamic radius (R_H) of the protein decreases upon the addition of EDTA in samples pretreated with $CaCl_2$.

Condition	R_H	Pd[a]	Mass
	nm	%	%
I (25 mM $CaCl_2$)	6.5	9.7	83.6
II (I + 50 mM EDTA)	3.1	11.9	99.6

[a] Pd, polydispersity.

Table 2

DLS analysis of *Lb*Prx1m pretreated with several divalent cations

Samples were pretreated with several divalent cations (at 20 mM) in 25 mM Tris-HCl (pH 7.5) and 5 mM EDTA. Note that only the additives $CaCl_2$ and $MgCl_2$ led to a monodisperse protein size distribution (Pd < 20%) in which most of the enzyme population (≥80% mass) displayed an average R_H (~6 nm) compatible with the decameric structure (R_G = 5 nm). Zn^{2+}, in particular, induced the formation of larger aggregates besides the species of R_H ~ 9 nm, probably because of non-specific interactions with the enzyme.

Salt	R_H	Pd[a]	Mass
	nm	%	%
$CaCl_2$	5.9	8.0	90
$MgCl_2$	5.6	10.1	80
$NiCl_2$	6.0	30.9	55
$FeCl_2$	4.6	29.3	50
$MnCl_2$	4.6	86.4	25
$ZnCl_2$	9.2	11.9	10

[a] Pd, polydispersity.

To study the effect of increasing concentrations of Ca^{2+} and Mg^{2+} in the dimer-decamer equilibrium of *Lb*Prx1m, we monitored changes in the oligomerization state of oxidized samples titrated with $CaCl_2$ or $MgCl_2$ by measuring the anisotropy of intrinsic protein fluorescence (Fig. 1*d*). Based on these data, we estimated a $K_{½}$ near 3 mM for both ions, indicating a low-affinity system. During these assays, we noticed that the cation effect was dependent on a critical protein concentration (~80 μM) below which oxidized *Lb*Prx1m dimers became less sensitive to the presence of cation (data not shown). However, after the formation of cation-stabilized decamers, the protein dilution to levels below the critical concentration did not induce decamer disassembly, indicating that cation binding to *Lb*Prx1m involves the formation of "transitional" decamers followed by the binding of Ca^{2+} or Mg^{2+} to yield stable cation-decamer complexes.

As a first approach to evaluating the physiological relevance of the Ca^{2+}/Mg^{2+} effect in the quaternary structure of *Lb*Prx1m, we performed aSEC assays under two conditions: first by simulating mitochondrial basal concentrations of free Mg^{2+} and Ca^{2+} ions (25, 26) and then by mimicking a Ca^{2+} increase to levels already reported for the *L. braziliensis* mitochondrion (27). Basal concentrations of Mg^{2+}/Ca^{2+} were sufficient to maintain most of the reduced enzyme in the decameric form, indicating that physiological levels of Mg^{2+}/Ca^{2+} stabilize reduced decamers (Fig. 1, *e* and *f*). We next exposed the cation-stabilized, reduced decamers to a low concentration of H_2O_2 and evaluated the aSEC profile of the oxidized (S–S-bonded) enzyme. In basal concentrations of Mg^{2+}/Ca^{2+}, most of the decamers dissociate into dimers upon C_p oxidation/resolution (Fig. 1, *e* and *f*), which correlates with the low affinity of these cations to the oxidized enzyme (Fig. 1*d*). However, under the condition simulating a calcium overload, almost half of the population remained decameric, indicating that supraphysiological Ca^{2+} concentration already reported for *Leishmania* mitochondria can increase the level of oxidized decamers (Fig. 1*e*).

Prx1m decamer stabilization by Ca^{2+}/Mg^{2+} is redox-independent and a unique feature of the mitochondrial Prx1 from Leishmania parasites

To further investigate how the redox state affects the oligomerization of *Lb*Prx1m, the hydrodynamic behavior of oxidized and reduced proteins was assessed under chelating conditions or in the presence of Ca^{2+} (Fig. 2). The aSEC results indicate that when the cation is absent the dimer-decamer equilibrium becomes more responsive to the protein redox state; the oxidized enzyme remains dimeric, regardless the protein concentration (Fig. 2*a*), whereas the reduced enzyme gets into a dimer-decamer equilibrium that is shifted to the decamer by increasing protein concentrations (Fig. 2*b*). In contrast, 25 mM $CaCl_2$ stabilizes a major population of oxidized and reduced decamers even when they are diluted to low protein concentrations (Fig. 2, *c* and *d*), supporting the conclusion that the Ca^{2+} effect surpasses the redox state in stabilizing *Lb*Prx1m decamers.

Unlike *Lb*Prx1m, the cytoplasmic 2-Cys Prx from the same pathogen, as well as from two evolutionarily distant organisms, were not as dependent as *Lb*Prx1m on the decamer-stabilizing effect of Ca^{2+}, eluting mainly as decamers regardless the presence of this ion or EDTA (Fig. 3). These findings indicate that the high sensitivity of dimer-decamer equilibrium to Ca^{2+}/Mg^{2+} ions is a unique feature of *Lb*Prx1m and possibly of other mitochondrial orthologues from *Leishmania* spp, according to the comparative structural and sequence analyses described below.

Structural basis for the cation-dependent mechanism of decamer stabilization

Despite extensive efforts, we were unable to crystallize *Lb*Prx1m in complex with Ca^{2+}. Crystals of *Lb*Prx1m decamers prestabilized with $CaCl_2$ were observed only under acidic conditions (pH 4.4), known to enhance decamer stability in a cation-independent manner (9) and to decrease the Ca^{2+}-binding affinity to proteins (28, 29). Thus, to determine the Ca^{2+}/Mg^{2+}-binding site in *Lb*Prx1m, we analyzed the crystal structure of the pH-stabilized decamer (PDB accession no. 4KB3 (9)) and used in *in silico* approaches combined with site-directed mutagenesis to validate the predicted site.

Like other members of the AhpC/Prx1 subfamily (30), the *Lb*Prx1m decamer is formed when five dimers bind to each other via the A-type interface (9). Because the formation of this interface depends on conformational changes in region I (residues 75–79) preceding the C_p-loop (residues 80–84) (9), we hypothesized that the decamer-stabilizing effect of Ca^{2+}/Mg^{2+} might be related to their binding to the A-type interface and the concomitant stabilization of region I in a conformation that favors the decameric assembly.

To test this hypothesis, we searched in the A-type interface of *Lb*Prx1m decamer (9) for negatively charged cavities in which a positive ion such as Ca^{2+} could bind and maintain the closed

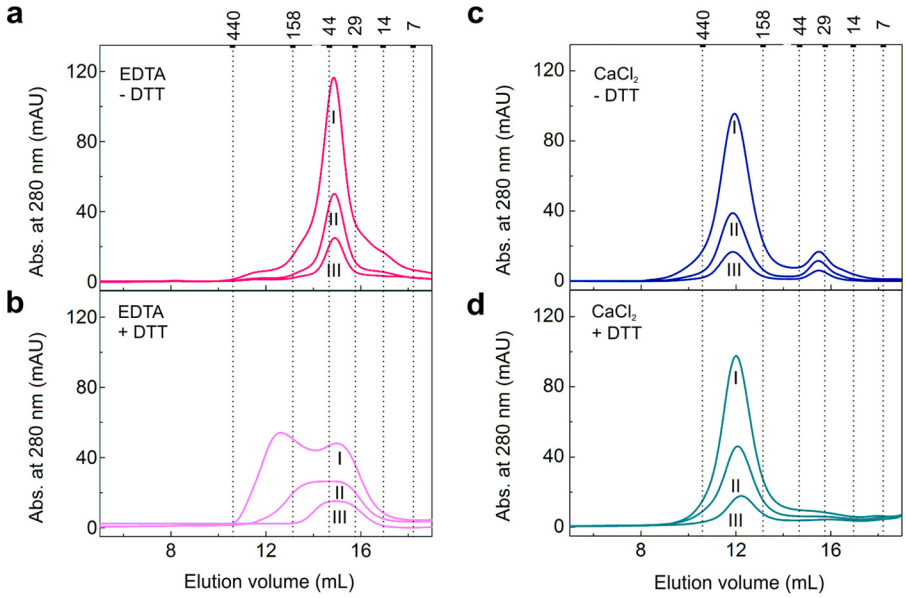

Figure 2. Ca^{2+} stabilizes both oxidized and reduced *Lb*Prx1m decamers. aSEC chromatograms of *Lb*Prx1m at different concentrations in Tris buffer (pH 7.5) containing 5 mM EDTA (*a*), 5 mM EDTA with 10 mM DTT (*b*), 25 mM $CaCl_2$ (*c*), or 25 mM $CaCl_2$ with 10 mM DTT (*d*). *Roman numerals* represent the protein concentration of the input samples (250 μl): *I*, 94 μM; *II*, 23 μM; *III*, 9 μM. *Numbers* above the graphs represent the molecular mass (kDa) of standard proteins used for column calibration. For this assay, the His tag was removed, using TEV protease to show that the untagged protein behaves similar to the His-tagged samples upon $CaCl_2$ and EDTA treatments (see Fig. 1*a*). Note that the Ca^{2+}-stabilized decamers, preformed at 94 μM protein, did not dissociate upon protein dilution even in the absence of DTT. Samples not treated with DTT are air-oxidized (S–S-bonded). *mAU*, milliabsorbance units.

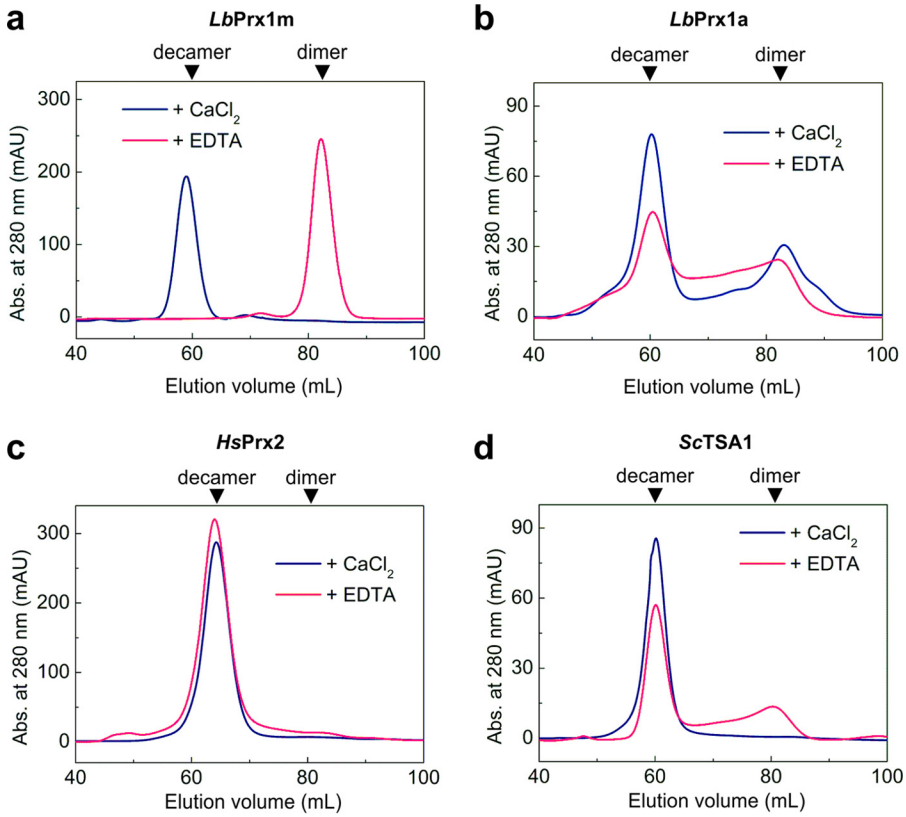

Figure 3. Decamer stabilization of cytoplasmic 2-Cys Prx from *Leishmania* and some distantly related homologues is Ca^{2+}-independent. SEC chromatograms of air-oxidized *Lb*Prx1m at 130 μM (*a*), cytoplasmic Prx1 from *L. braziliensis* (*Lb*Prx1a) at 43 μM (*b*), human Prx2 at 130 μM (*c*), and yeast *TSA1* at 43 μM (*d*) loaded (2 ml) into a HiLoad Superdex 200 16/600 column pre-equilibrated with Tris buffer (pH 7.5) containing 25 mM $CaCl_2$ or 5 mM EDTA. *mAU*, milliabsorbance units.

conformation of region I required for decamer stabilization (9). As expected, we found a site in which Ca^{2+} could be coordinated by residues from both interfacing subunits, assuming a distorted trigonal bipyramidal geometry according to molecular dynamics simulations (Fig. 4*a*). This site includes the main chain of Asp-76, a residue from region I, and is duplicated at each A-type interface, implying a stoichiometry of 10 cations/decamer.

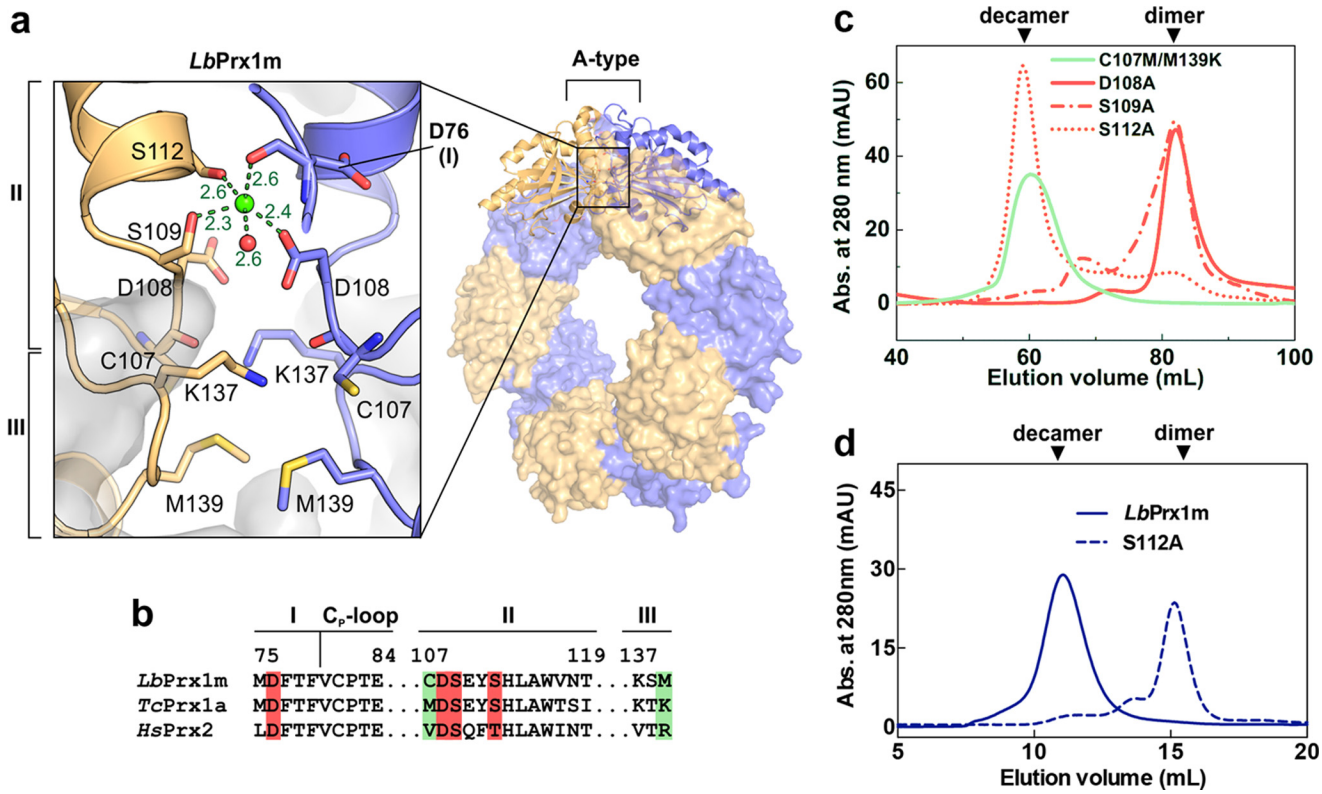

Figure 4. Structural basis for the Ca^{2+}/Mg^{2+}-dependent decamerization of *Lb*Prx1m. *a*, magnified view of the A-type interface from *Lb*Prx1m crystal structure (PDB accession no. 4KB3) after molecular dynamics simulations in the presence of Ca^{2+} (*green sphere*). Interfacing subunits are shown in *orange* and *violet*. For purposes of clarity, we named the A-type interface regions according to the nomenclature proposed by Wood *et al.* (15) (regions I–III). Shown as sticks are the residues involved in the cation-dependent mechanism of decamer stabilization: Asp-76, region I; Cys-107, Asp-108, Ser-109, and Ser-112, region II; Lys-137 and Met-139, region III. *b*, sequence alignment of A-type interface regions from *Lb*Prx1m and two cation-independent 2-Cys Prx, highlighting the residues predicted to play a role in cation binding (*red boxes*) and those predicted to determine the cation dependence of decamer stabilization (*green boxes*). *c*, aSEC chromatograms of air-oxidized *Lb*Prx1m D108A, S109A, S112A, and C107M/M139K mutants at 86 μM (500 μl) in Tris buffer (pH 7.5) containing 25 mM $CaCl_2$ (*red lines*) or 5 mM EDTA (*green line*). The single mutant C107M was unstable in solution, and thus it was not included in our analyses. *mAU*, milliabsorbance units. *d*, aSEC chromatogram of air-oxidized *Lb*Prx1m WT and S112A mutant at 13 μM (200 μl). Note that WT protein eluted as decamer, whereas the S112A mutant eluted mainly as dimer under the same conditions. aSEC assays were carried out in Tris buffer (pH 7.5) containing 25 mM $CaCl_2$.

We next evaluated the Ca^{2+} effect on the aSEC profile of mutants lacking one of the side chains predicted to coordinate this cation. These side chains belong to the residues Asp-108, Ser-109, and Ser-112, located in region II (residues 107–120) of the A-type interface (Fig. 4). The mutants D108A and S109A eluted essentially as dimers in the presence of Ca^{2+} at pH 7.5, whereas mutant S112A showed a concentration-dependent behavior, eluting as a decamer at 86 μM and as a dimer at 13 μM (Fig. 4, *c* and *d*). These results indicate that Asp-108 and Ser-109 are essential for the Ca^{2+}-dependent stabilization of the *Lb*Prx1m decamer, whereas Ser-112 plays a facultative role in this mechanism.

Intriguingly, the cation-binding site identified in *Lb*Prx1m is highly conserved in some 2-Cys Prx, where the decamers remain stable without Ca^{2+}/Mg^{2+} ions, such as the cytoplasmic peroxiredoxin from *Trypanosoma cruzi* (*Tc*Prx1a) in which the decamer is crystallized in the presence of EDTA (31) and human Prx2 (*Hs*Prx2) (Fig. 4*b*). This finding prompted us to search for other structural elements that would possibly account for the Ca^{2+}/Mg^{2+} effect on *Lb*Prx1m.

A comparison of the A-type interfaces of the *Lb*Prx1m, *Tc*Prx1a, and *Hs*Prx2 crystallographic decamers (Fig. 5) showed that residues Cys-107 and Met-139 are exclusive of *Lb*Prx1m and expose Asp-108 to the electrostatic attraction of Lys-137 (Fig. 5*a*). However, in *Tc*Prx1a, the Asp-108 counterpart (Asp-79) is shielded from the influence of such a lysine by a residue that is bulkier than Cys-107 (Met-78), which seems to favor the interaction between the Asp-79 side chain and a water molecule that occupies the predicted cation-binding site (Fig. 5*b*). The same water-mediated link occurs in *Hs*Prx2, which lacks the corresponding Lys-137 (Fig. 5*c*). Thus, we hypothesized that the attraction of the Asp-108 side chain by Lys-137 prevents Asp-108 from coordinating a water molecule, but not a Ca^{2+} or Mg^{2+} ion, within the Ser/Asp cluster, destabilizing the A-type interface when Ca^{2+} or Mg^{2+} is absent and the medium is alkaline (9). To test this hypothesis, we mutated Cys-107 (region II) to a methionine and Met-139 (region III) to a lysine, thus mimicking the *Tc*Prx1a Asp-79 (equivalent to Asp-108) microenvironment in which Met-78 blocks the access of the lysine to the aspartate (Fig. 5*b*). As envisioned, this double mutation rendered *Lb*Prx1m decamer stabilization Ca^{2+}-independent (Fig. 4*c*), demonstrating that changes in regions II and III of the A-type interface gave rise to the Ca^{2+}/Mg^{2+} effect on *Lb*Prx1m oligomerization (Fig. 5*a*).

Ca^{2+}/Mg^{2+} ions enhance the peroxidase activity of LbPrx1m

The dimer-decamer switch seems to play a role during the peroxidase catalytic cycle of AhpC/Prx1 subfamily members by

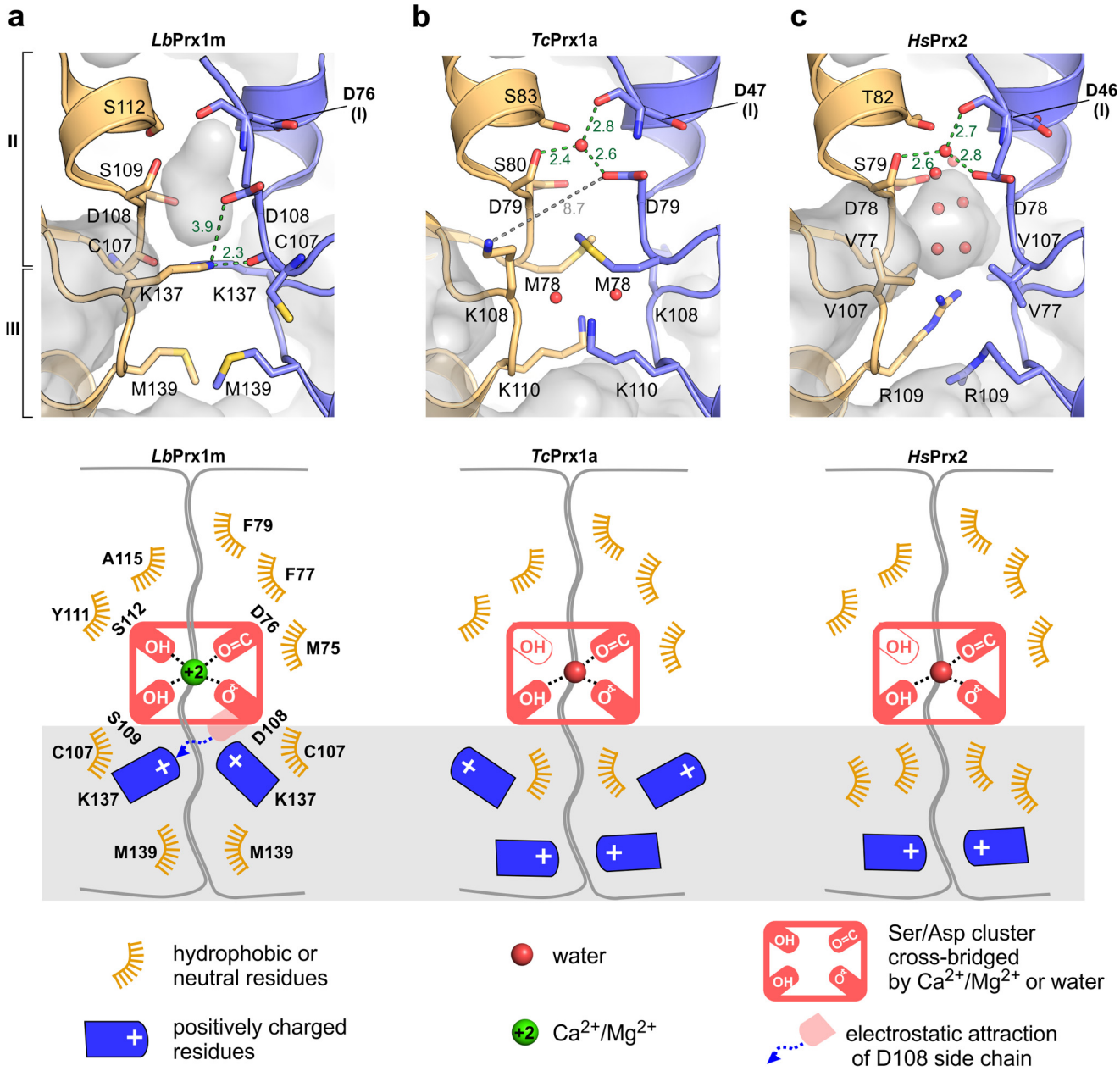

Figure 5. Structural comparison of the A-type interface between *Lb*Prx1m (*a*), *Tc*Prx1a (PDB accession no. 4LLR) (*b*), and human Prx2 (PDB accession no. 1QMV) (*c*) reveals the molecular determinants for calcium specificity in *Lb*Prx1m. *Green* or *gray dashed lines* indicate interatomic distances labeled in Å, and *red spheres* represent water molecules. In *b*, note the long distance between the Asp-79 and Lys-108 side chains, indicating they do not interact in the *Tc*Prx1a structure. *Below* each panel there is a schematic representation of the A-type interface of *Lb*Prx1m, *Tc*Prx1a, and human Prx2 that highlights the changes observed in regions II and III (*gray box*), which determine the Ca^{2+} dependence of *Lb*Prx1m decamerization at physiological pH.

influencing enzymatic efficiency (15, 32). We thus used the trypanothione-dependent enzyme cascade from *Leishmania* to evaluate *in vitro* how the decamer-stabilizing effect of Ca^{2+}/Mg^{2+} influences the capability of *Lb*Prx1m to reduce hydrogen peroxide.

The chelation of metal ions drastically decreased the peroxidase activity of purified *Lb*Prx1m (Fig. 6*a*). In samples pretreated with EDTA and then supplemented with Ca^{2+} or Mg^{2+}, the catalytic activity was recovered, showing that these divalent cations play a role in the peroxidase function of *Lb*Prx1m (Fig. 6*a*). The increment of Ca^{2+} in purified *Lb*Prx1m did not alter its catalytic activity (Fig. 6*a*), an effect that can be ascribed to divalent cations from *Escherichia coli* that remained bound to *Lb*Prx1m decamers during the purification process, as indicated by aSEC analysis of untreated samples (results not shown). The observed effects of EDTA and Ca^{2+} cannot be attributed to interference from the other molecules of the trypanothione cascade, because these additives did not alter the peroxidase activity of cytoplasmic Prx1 from *L. infantum* (*Li*Prx1a) (Fig. 6*b*). Importantly, the observation that the Ca^{2+}/Mg^{2+} ions did not affect the peroxidase activity of *Li*Prx1a correlates with the fact that Ca^{2+}/Mg^{2+} ions are not required to stabilize the decameric structure of its ortholog in *L. braziliensis* (Fig. 3), corroborating our view of the spe-

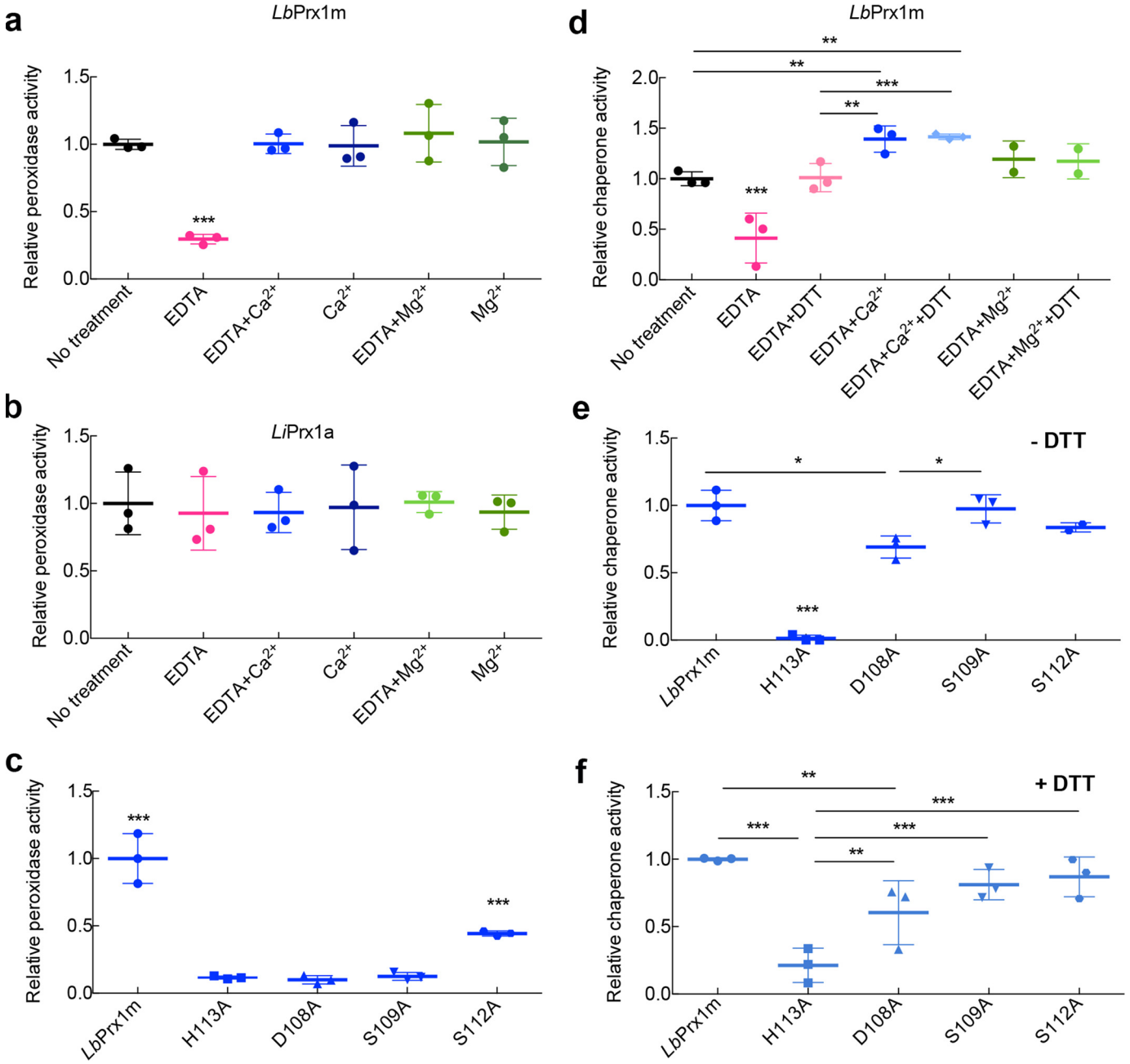

Figure 6. Ca^{2+} and Mg^{2+} ions enhance both peroxidase and chaperone activities of *Lb*Prx1m. *a*, relative peroxidase activity of *Lb*Prx1m left untreated, pretreated with 5 mM EDTA only, pretreated with 5 mM EDTA followed by the addition of 25 mM $CaCl_2$ or $MgCl_2$, and pretreated with 20 mM $CaCl_2$ or $MgCl_2$ alone. *b*, relative peroxidase activity of *Li*Prx1a prepared as described for *Lb*Prx1m. The absolute peroxidase activity values (μmol NADPH·min^{-1}·mg^{-1}) were 0.18 ± 0.04 (for untreated *Lb*Prx1m) and 5.12 ± 1.19 (for untreated *Li*Prx1a). *c*, comparison between the relative peroxidase activity of WT *Lb*Prx1m and mutants pretreated with 5 mM EDTA followed by the addition of 25 mM $CaCl_2$. *d*, relative chaperone activity of air-oxidized *Lb*Prx1m left untreated and pretreated with 5 mM EDTA only or 5 mM EDTA followed by the addition of 25 mM $CaCl_2$ or $MgCl_2$. The same treatments were carried out with the protein reduced using 2 mM DTT. *e* and *f*, comparison between the relative chaperone activity of WT *Lb*Prx1m and muteins pretreated with 5 mM EDTA followed by the addition of 25 mM $CaCl_2$ without DTT (air-oxidized) (*e*) or with 2 mM DTT (reduced) (*f*). *, $p < 0.1$; **, $p < 0.05$; ***, $p < 0.01$. All experiments were performed in triplicate.

cific effect of Ca^{2+}/Mg^{2+} on the peroxidase activity of the *Leishmania* mitochondrial enzyme.

To demonstrate that the effect of Ca^{2+} on peroxidase activity is due to its binding at the A-type interface and consequent decamer stabilization, we compared the peroxidase activity of Ca^{2+}-binding site mutants with that of the wild-type (WT) protein or the mutant H113A (Fig. 6, *a–c*), which preserves the dimeric structure but is unable to decamerize in response to pH (9), redox, and cation stimuli (Fig. 7*a*). Mutants D108A and S109A displayed only residual activity compared with the WT enzyme in the presence of Ca^{2+} (Fig. 6*c*). As expected, the mutation S112A was not as efficient as the D108A and S109A substitutions in decreasing the peroxidase activity of *Lb*Prx1m, which correlates with the facultative role of Ser-112 in Ca^{2+} binding. The effects of the D108A and S109A mutations on peroxidase activity were equivalent to that caused by the decamer-disrupting H113A substitution, further

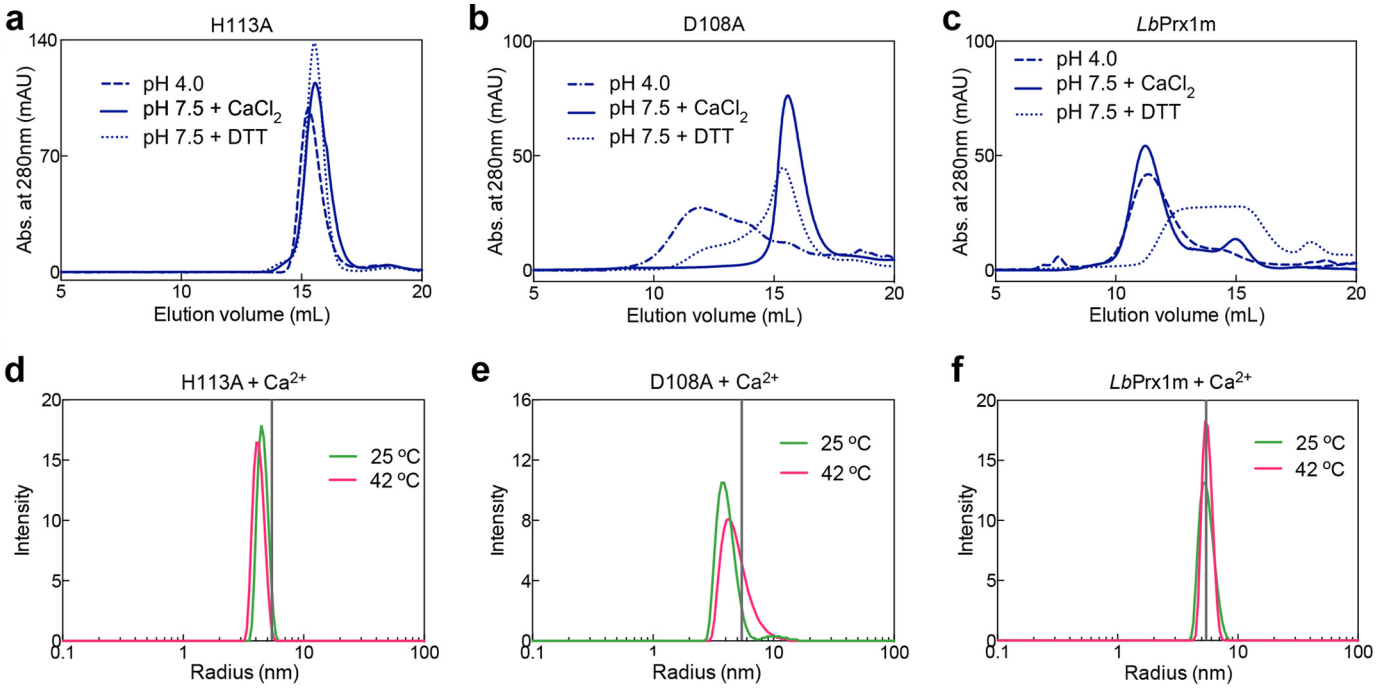

Figure 7. The influence of low pH, $CaCl_2$, DTT, or temperature on the hydrodynamic behavior of the mutants H113A and D108A and WT *Lb*Prx1m. aSEC assays of H113A (*a*), D108A (*b*), and WT *Lb*Prx1m (*c*) were carried out with proteins at 48 μM (250 μl) in MMT buffer (pH 4.0) and 10 mM EDTA (*dashed-dotted line*), Tris buffer (pH 7.5) and 25 mM $CaCl_2$ (*solid line*), or Tris buffer (pH 7.5) and 5 mM EDTA containing 2 mM DTT (*dotted line*). Chromatograms of mutant H113A and *Lb*Prx1m at pH 4.0 as well as *Lb*Prx1m at pH 7.5 plus 2 mM DTT were shown previously (9) and are represented here for comparison purposes. DLS analyses at 25 and 42 °C of H113A (*d*), D108A (*e*), and WT *Lb*Prx1m (*f*) were performed with protein samples at 100 μM pretreated with 5 mM EDTA followed by the addition of 25 mM $CaCl_2$ in Tris buffer (pH 7.5). The *vertical gray lines* represent the mean radius estimated for WT *Lb*Prx1m decamers. Samples not treated with DTT are air-oxidized (S–S-bonded). *mAU*, milliabsorbance units.

supporting that Ca^{2+}/Mg^{2+} ions enhance *Lb*Prx1m peroxidase activity by stabilizing its decameric form.

Reduced and oxidized cation-stabilized decamers possess the required conformation to perform chaperone function

Our finding that Ca^{2+}/Mg^{2+} ions stabilize oxidized decamers of *Lb*Prx1m led us to investigate whether these decamers were able to suppress luciferase thermal aggregation similarly to the reduced decamers (3). Under non-reducing conditions, metal chelation inhibited the chaperone activity of *Lb*Prx1m, indicating a role for Ca^{2+}/Mg^{2+} in activating the chaperone function of oxidized *Lb*Prx1m (Fig. 6*d*). When cation-free samples were supplemented with $CaCl_2$ or $MgCl_2$, the chaperone activity was recovered, reaching levels significantly higher than that of the untreated samples in the case of Ca^{2+} (Fig. 6*d*). Although *Lb*Prx1m reduction also rescued the chaperone activity of cation-free *Lb*Prx1m, the average activity of the reduced decamers was further stimulated by $CaCl_2$ supplementation (Fig. 6*d*), which is in agreement with aSEC data showing the better performance of Ca^{2+} than protein reduction in stabilizing decamers (Fig. 2).

To demonstrate that protection against luciferase aggregation depends on the formation of decamers and to evaluate the effect of Ca^{2+}/Mg^{2+}-binding site mutations on chaperone function, we measured the chaperone activity of *Lb*Prx1m mutants H113A, D108A, S109A, and S112A. The H113A substitution, which prevents the decameric assembly of dimers, completely abolished the chaperone activity of oxidized *Lb*Prx1m and drastically decreased that of the reduced protein, demonstrating that decamer formation is a prerequisite for chaperone activity (Fig. 6, *e* and *f*). Unexpectedly, of the four Ca^{2+}-binding site mutations, only D108A significantly decreased the chaperone activity under both non-reducing and reducing conditions (Fig. 6, *e* and *f*). However, the mutant D108A was more active than H113A, which prompted us to investigate whether the high temperature of the chaperone assay favors the formation of D108A decamers. In agreement with the chaperone activity data, mutant D108A entered into a dimer-decamer equilibrium at 42 °C (Fig. 7, *b* and *e*), whereas mutant H113A remained in the dimeric state at this temperature (Fig. 7, *a* and *d*). Under the same conditions, the WT protein was decameric, indicating that decamer formation is necessary and sufficient to trigger the chaperone function of *Lb*Prx1m (Fig. 7, *c* and *f*).

Based on studies of reduced decamers, it has been proposed that the chaperone function of *Leishmania* Prx1m is activated by an increase in temperature, which induces conformational rearrangements that expose hydrophobic regions (3). As our data showed that oxidized decamers also display chaperone activity, we investigated whether their behavior upon temperature increase supports the model in which thermo-induced conformational changes activate the chaperone function of *Leishmania* Prx1m. For this purpose, circular dichroism (CD) spectra of WT *Lb*Prx1m were collected under reducing and non-reducing conditions at 25 and 42 °C in the presence of Ca^{2+}. Interestingly, at 25 °C, the CD spectra of the reduced and oxidized decamers were virtually identical, showing that the conformational differences between their respective fully folded and locally unfolded active sites were undetectable by

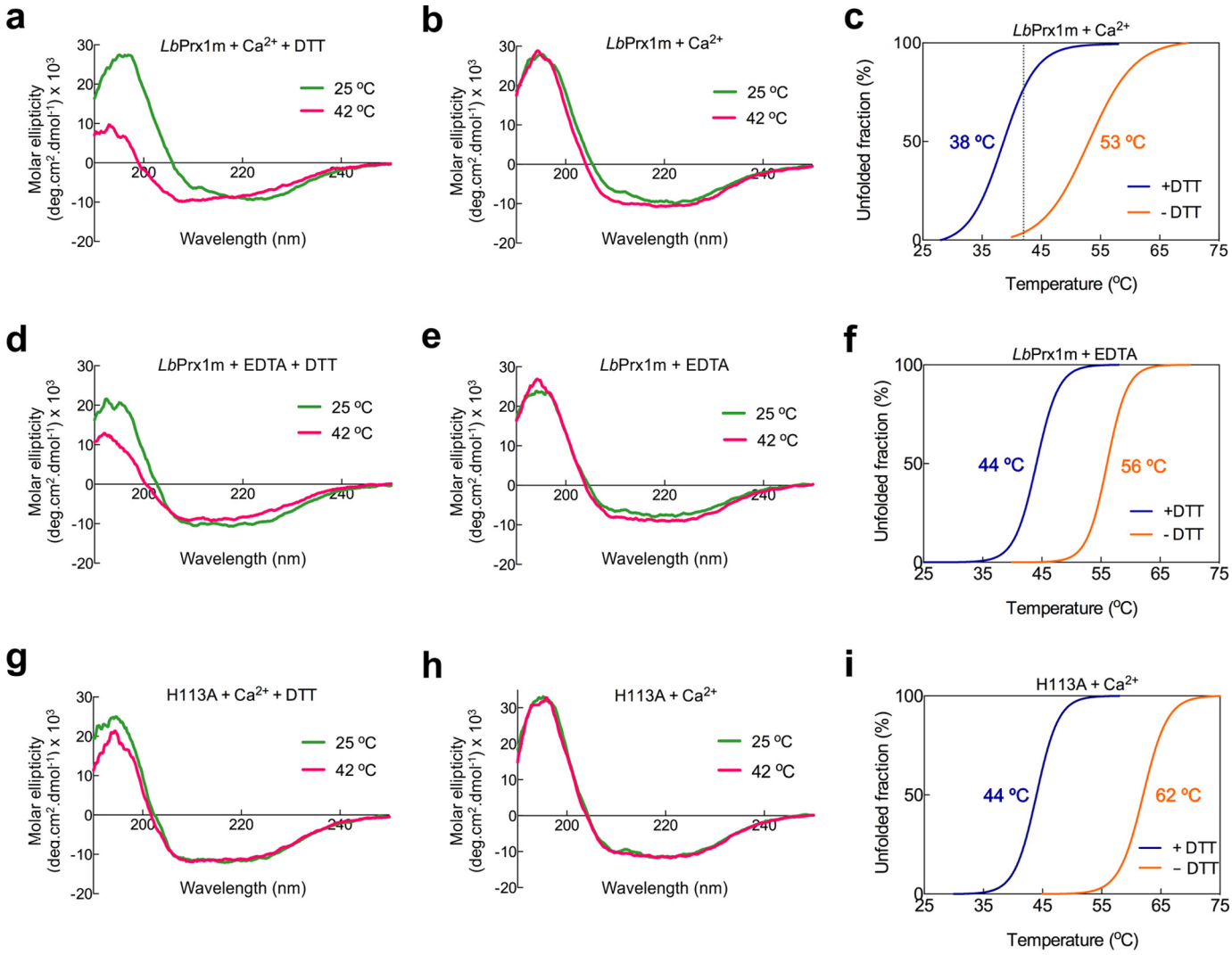

Figure 8. Biophysical analyses of *Lb*Prx1m dimers and decamers. Circular dichroism spectra of WT *Lb*Prx1m or mutant H113A pretreated with 5 mM EDTA followed by the addition of 25 mM $CaCl_2$ and 2 mM DTT (*a* and *g*), 25 mM $CaCl_2$ only (S–S-bonded) (*b* and *h*), 2 mM DTT only (*d*), or without further additives (air-oxidized) (*e*) at 25 °C (*green*) and 42 °C (*pink*). Shown are DSF data of reduced (+DTT) or air-oxidized (−DTT) *Lb*Prx1m (*c* and *f*) as well as mutant H113A (*i*) treated as described for the CD experiments. In these assays, WT *Lb*Prx1m data in the presence of Ca^{2+} reflect the CD and DSF profiles of decamers, whereas those of WT *Lb*Prx1m in the presence of EDTA or those of the mutant H113A represent the behavior of the dimers. The calculated melting temperatures are color-coded according to the respective curves. In *c*, note that the *dashed line* indicates the temperature of the chaperone assay in which the reduced decamers expose hydrophobic patches, whereas the oxidized decamers remain almost completely folded.

this technique (Fig. 8, *a* and *b*). Upon a temperature increase from 25 to 42 °C, the CD spectrum of the reduced decamers showed a decrease in the absolute values at 193 and 222 nm and presented a shift of the minimum at 208 nm toward smaller wavelengths, indicating the loss of α-helical structures (Fig. 8*a*). In agreement with this result, differential scanning fluorimetry (DSF) data showed the exposure of hydrophobic surfaces in reduced decamers heated up to 42 °C (Fig. 8*c*). However, no significant changes in CD spectra or exposure of hydrophobic regions in DSF analyses were observed for the oxidized decamers in the same temperature range (Fig. 8, *b* and *c*). This enhanced thermostability of the oxidized species correlates with the presence of the disulfide bond linking C_p, located in the loop connecting strand β3 to helix α2, and C_r, placed at the C-terminal extension downstream the helix α6. Because this is the only disulfide bond present in oxidized *Lb*Prx1m (9), the loss of structure indicated by CD and DSF analyses of reduced decamers likely reflects, among other events, the unfolding of helices α2 and/or α6, which is favored when C_p and C_r are reduced.

Considering that the helices α2 and α6 are located at the external surface of the decamer, *i.e.* far from the luciferase-binding site (3), their unfolding might not interfere with the chaperone function of reduced decamers (Fig. 9). In support of this hypothesis, the Ca^{2+}-stabilized reduced species preserved the decameric structure at 42 °C (data not shown) and were as effective as the oxidized samples in suppressing the thermal aggregation of luciferase *in vitro* (Fig. 6*d*). Together, these analyses suggest that the thermo-induced conformational changes observed for the reduced decamer might not be required to activate the chaperone function of *Leishmania* Prx1m.

For comparison purposes, we also performed CD and DSF analyses for the WT *Lb*Prx1m in presence of EDTA, a condition that favors the dimeric state, and the mutant H113A, which is fully dimeric in solution regardless of its redox state (Fig. 8, *d–i*).

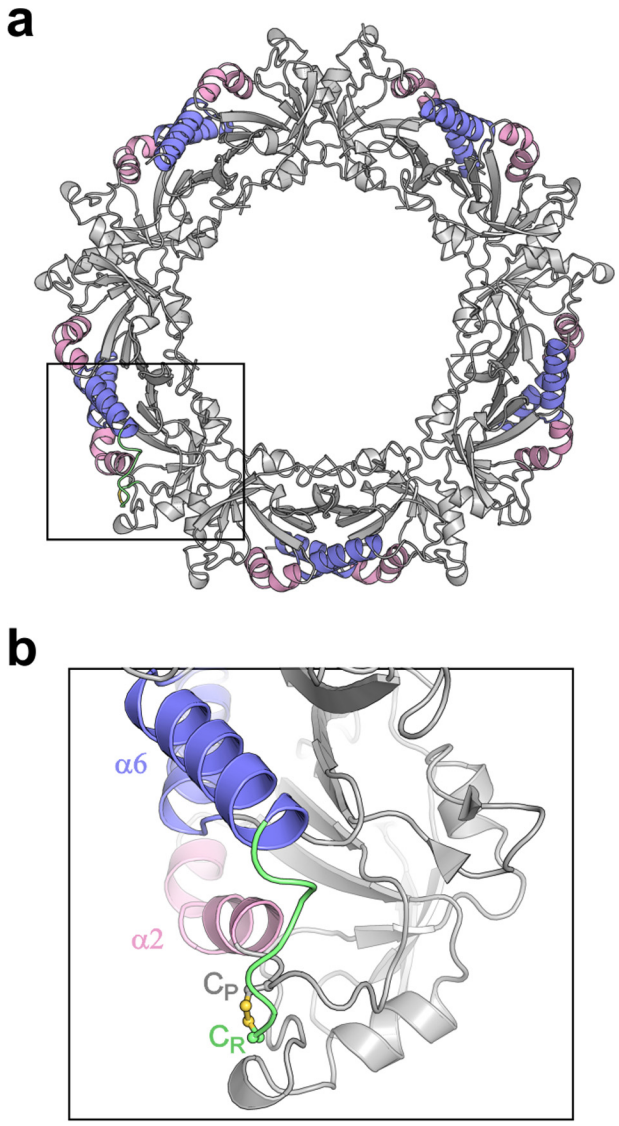

Figure 9. The disulfide bond between C_p and C_r probably suppresses the unfolding of helices α2 and or α6 at 42 °C. *a*, schematic representation of *Lb*Prx1m crystallographic decamer highlighting helices α2 (*pink*) and α6 (*violet*). *b*, magnified view of the *boxed region* in *a*, showing the disulfide bond between C_p (*gray*, carbon atoms) and C_r (*green*, carbon atoms). The C-terminal extension harboring C_r is shown in *green*.

These experiments confirmed that the mutant H113A is properly folded (Fig. 8, *g* and *h*) and revealed that the C_pS–SC_r disulfide bond has a higher impact in thermostability than variations in the oligomeric state, leading to an increase of at least 12 °C in the melting temperature of both the dimers and the decamers (Fig. 8, *c*, *f*, and *i*).

Preventing Prx1m decamer formation impairs leishmanial survival at 37 °C

Previous work has shown that *L. infantum* parasites devoid of *Li*Prx1m are thermosensitive when exposed to 37 °C, a phenotype that is partially reverted upon reintroduction of the enzyme (2). To investigate the phenotypic implications of Prx1m mutants unable to decamerize or with a lesser tendency to form Ca^{2+}/Mg^{2+}-stabilized decamers, *L. infantum* knock-out parasites for *Li*Prx1m (*prx1m*$^-$) were transfected with WT *Lb*Prx1m and the corresponding H113A and D108A muteins. Using indirect immunofluorescence (Fig. 10*a*), Western blotting (Fig. 10*b*), and PCR (data not shown) analyses, it was verified that knock-out parasites lacked the expression of *Li*Prx1m, whereas the transfected parasites expressed the WT protein and mutants into the mitochondrion.

As expected, at 25 °C, all parasites had the same growth rates (Fig. 10*c*). However, at 37 °C, the H113A dimers were incapable of rescuing the thermosensitive phenotype of *Prx1m*$^-$ *promastigotes*, demonstrating that the decameric state of Prx1m is crucial for *Leishmania* survival at temperatures akin to those encountered in the mammalian host (Fig. 10, *d* and *e*).

When exposed to 37 °C, knock-out parasites expressing the D108A mutein, which is less prone to form Ca^{2+}/Mg^{2+}-stabilized decamers, presented a behavior similar to those complemented with the WT protein (Fig. 10, *d* and *e*). This result is likely explained by the fact that the chaperone activity of this mutant retains a residual response to Ca^{2+} (Fig. 10*f*). Furthermore, mutant D108A is susceptible to the influence of medium acidification, which stabilizes a subpopulation of D108A as decamers *in vitro* (Fig. 7*b*) and probably counterbalances the lower responsiveness of D108A decamers to Ca^{2+}/Mg^{2+} *in vivo*. Interestingly, the chaperone activity of the mutant D108A *in vitro* is unresponsive to DTT treatment even under cation-free conditions (Fig. 10*f*), indicating that decamer-stabilizing factors other than protein reduction support the chaperone function of this mutein *in vivo*.

Discussion

Ca^{2+}/Mg^{2+} ions stabilize decamers and activate the dual function of mitochondrial 2-Cys Prx from Leishmania parasites

In this work, we have revealed that Ca^{2+} and Mg^{2+} ions affect the quaternary structure and the dual function of mitochondrial 2-Cys peroxiredoxins from *Leishmania* parasites. Our data show that these divalent cations stabilize *Lb*Prx1m decamers and thereby stimulate peroxidase and chaperone activities. The mechanism involves the binding of Ca^{2+} or Mg^{2+} at transitional A-type interfaces, stabilizing dimer-dimer interactions. Although the $K_{½}$ estimated for Ca^{2+} and Mg^{2+} binding was near 3 mM for the oxidized enzyme, our analyses suggest that this affinity can be enhanced by protein reduction, which stabilizes transitional decamers and favors the formation of cation-bound decamers. Supporting this hypothesis, air-oxidized samples treated with EDTA and then incubated with 1 mM Ca^{2+} behaved essentially as dimers (Fig. 1*d*); however, when these EDTA-treated samples were reduced with DTT, incubated with similar amounts of cation, and then reoxidized, about 50% of the enzyme remained in the decameric form (Fig. 1, *e* and *f*). In other words, the amount of cation-bound oxidized decamers increases when these complexes are formed under reducing conditions prior to enzyme oxidation. In summary, our data indicate that physiological concentrations of free Ca^{2+}/Mg^{2+} stabilize reduced decamers, stimulating the peroxidase function and contributing to the maintenance of a basal pool of chaperone-active *Lb*Prx1m at the alkaline environment of mitochondria (pH 7.5–8.0) (33). When mitochondrial Ca^{2+} uptake is stimulated (23), the level of oxidized decamers in-

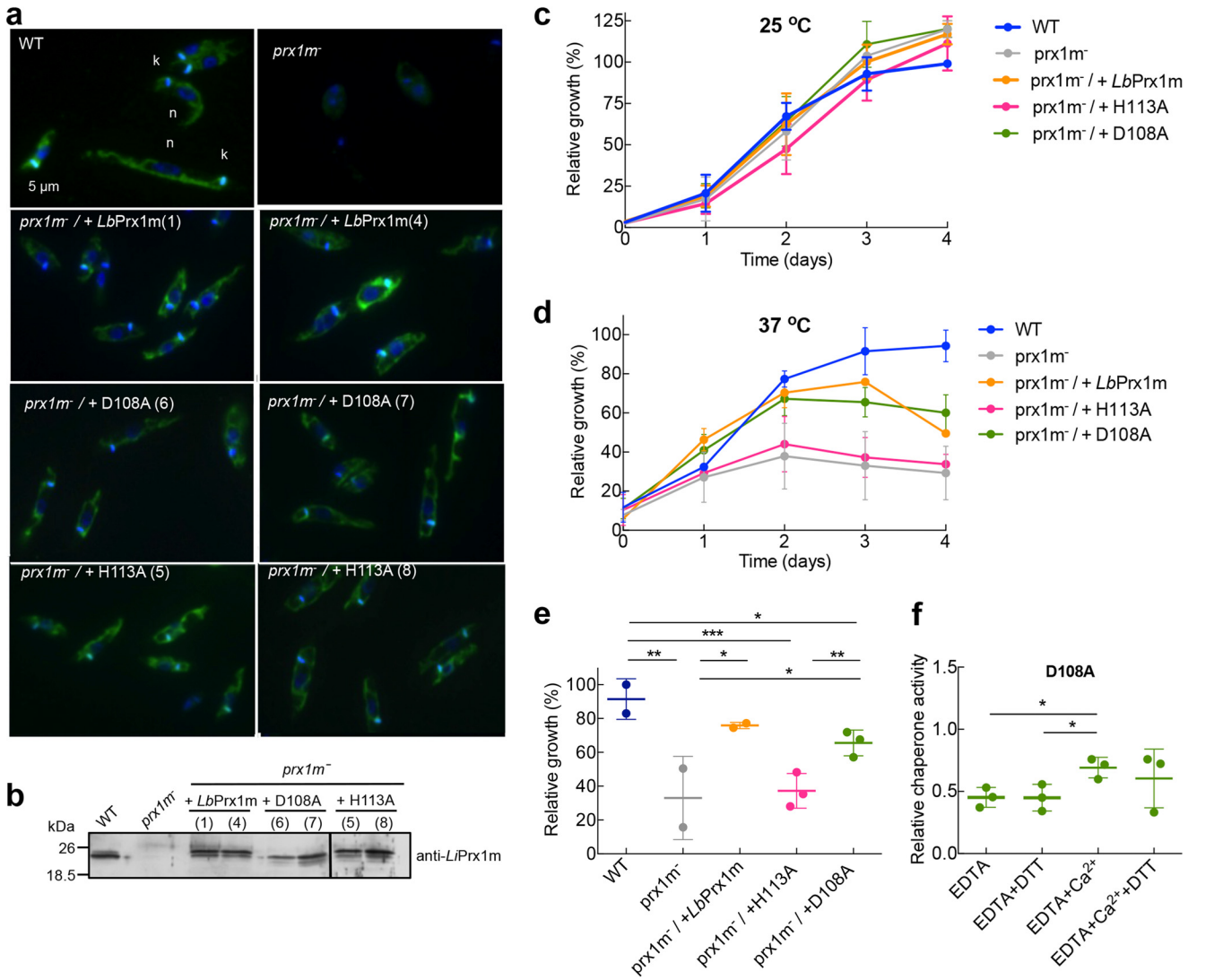

Figure 10. *Leishmania* growth at 37 °C depends on Prx1m decamerization. *a*, indirect immunofluorescence of *L. infantum* (WT), *L. infantum* knock-out for *Li*Prx1m (*prx1m*$^{-}$), and *prx1m*$^{-}$ complemented with *Lb*Prx1mH113A (clones 5 and 8), *Lb*Prx1mD108A (clones 6 and 7), and WT *Lb*Prx1m (clones 1 and 4). Parasites were incubated with anti-Prx1m antibody (*green*) and merged with DAPI (*blue*) (*n*, nucleus; *k*, kinetoplast). *b*, Western blotting analysis using anti-*Li*Prx1m antibody (53) of *L. infantum* WT, *prx1m*$^{-}$, and the transfectants. A total of 20 μg of protein extracts were loaded per lane. *Leishmania* growth curves at 25 °C (*c*) and 37 °C (*d*) for WT, *prx1m*$^{-}$, and transfectants. The experiments were performed in duplicate for *L. infantum* WT and *prx1m*$^{-}$ and in triplicate for the transfectants. *e*, statistical analysis of *Leishmania* relative growth at 37 °C considering the day 3 representation in *d*. *, $p < 0.1$; **, $p < 0.05$; ***, $p < 0.01$. *f*, *in vitro* chaperone activity of mutant D108A in the presence of 5 mM EDTA or 5 mM EDTA followed by the addition of 25 mM $CaCl_2$, with or without 2 mM DTT, in Tris buffer (pH 7.5) (*, $p < 0.1$). All experiments were performed in triplicate. Relative activities were calculated with respect to the activity of WT protein in the presence of Ca^{2+} or Ca^{2+} plus DTT according to the absence or presence of DTT in the tested condition. Samples not treated with DTT are air-oxidized (S–S-bonded).

creases, contributing to an enlarged chaperone reservoir of Prx1m in *Leishmania*.

The closed conformation of region I is required to stabilize the fully folded conformation of the reduced C_p-loop

According to data from the literature, the decameric structure of 2-Cys Prx contributes to stabilizing the fully folded conformation of the active site, allowing the optimal orientation of substrate and the activation of the catalytic C_p to reduce the peroxide oxygen (15, 32). Our data support the conception that for the C_p-loop to adopt the fully folded conformation, the adjacent region I might be stabilized in a closed conformation via interactions involving residue Asp-76 (Fig. 11). The disruption of such interactions by point mutations severely decreases the peroxidase activity of *LbPrx1m* (Fig. 6*c*). Although the link between the Asp-76 and His-113 side chains is intramolecular and direct, those involving the Asp-76 main chain require decamer assembly and are mediated by Ca^{2+} or Mg^{2+} ions in the case of *Lb*Prx1m (Fig. 11). Our data revealed that Mg^{2+} or Ca^{2+} ions increase the peroxidase activity by binding at the A-type interface of *Lb*Prx1m, thus holding the Asp-76 main chain with the assistance of Asp-108, Ser-109, and optionally Ser-112 side chains. Noticeably, mutations at positions 108 and 109 displayed a higher impact on peroxidase activity in comparison with EDTA treatment, suggesting that, in the absence of divalent cations, a solvent molecule could link this Ser/Asp cluster allowing a suboptimal activity. Indeed, in several members of the AhpC/Prx1 subfamily, from bacteria to mammals, a water molecule plays the role of linking the highly conserved Ser/Asp cluster at the A-type interface (Fig. 12).

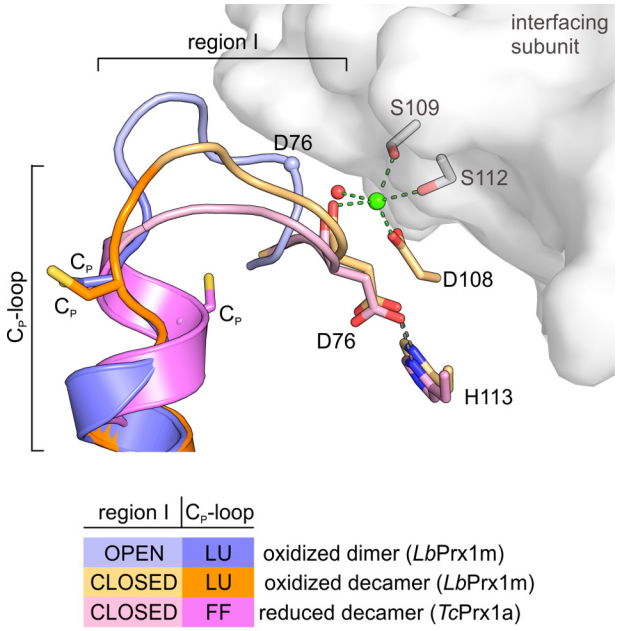

Figure 11. Stabilization of region I in the closed conformation is required to maintain the fully folded conformation of the C_P-loop upon C_P reduction. Shown is a 3D alignment of the loop-helix active-site motif (region I + C_P-loop) of *Lb*Prx1m-oxidized dimer (shades of *violet*; PDB accession no. 4KCE), *Lb*Prx1m-oxidized decamer (shades of *orange*; PDB accession no. 4KB3) after molecular dynamics simulations with Ca^{2+} bound (*green sphere*) at the A-type interface (*gray surface*), and reduced decamer *Tc*Prx1a (shades of *pink*; PDB accession no. 4LLR). Note that region I adopts an open conformation in dimers, but it assumes a closed conformation in the oxidized and reduced decamers. According to our data, the stabilization of region I in the closed conformation requires at least an H-bond between Asp-76 and His-113 as well as Ca^{2+} (*green sphere*), Mg^{2+}, or (less efficiently) the water molecule at the A-type interface. The establishment of such interactions is crucial to maintain the fully folded (*FF*) form of the reduced C_P-loop. In the *Lb*Prx1m dimer, the high entropy of the region I, trapped in an open conformation in chain B but disordered in chain A, might propagate to the adjacent C_P-loop, hampering the stabilization of fully folded conformation required for substrate binding and catalysis. *LU*, locally unfolded.

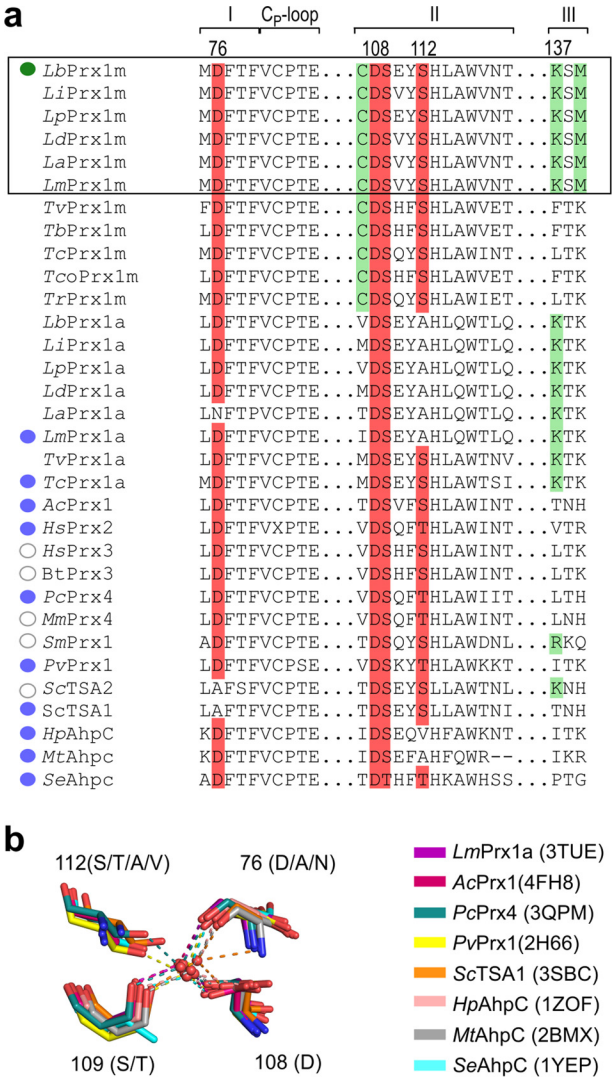

Figure 12. Stabilization of region I in the closed conformation is mediated by Ca^{2+}/Mg^{2+} in mitochondrial Prx1 from *Leishmania* species and by a water molecule in other AhpC/Prx1 subfamily members. *a*, sequence alignment of regions I, II, and III from the A-type interface as well as the C_P-loop from mitochondrial (Prx1m) and cytoplasmic (Prx1a) 2-Cys Prx from trypanosomatids with known crystallographic decamers. Note that residues involved in cation binding in *Lb*Prx1m are highly conserved in the AhpC/Prx1 subfamily (*red boxes*). However, only the mitochondrial enzymes from *Leishmania* (*black outlined* area) conserve residues Cys-107, Lys-137, and Met-139 (*green boxes*) that render decamer stabilization of *Lb*Prx1m highly sensitive to Ca^{2+} and Mg^{2+} ions (*green circle*). In other 2-Cys Prx, Lys-137 is replaced by neutral polar or hydrophobic residues or kept away from Asp-108 by residues bulkier than Cys-107. In most of the analyzed structures of AhpC/Prx1 subfamily members (*blue circles*), a water molecule mediates the link between the Asp-76 main chain and Asp-108, Ser-109, and eventually Ser-112 side chains. In a few cases, solvent molecules are not observed in the crystallographic structures due to the low resolution of data (*open circles*). *Lb*, *L. braziliensis*; *Li*, *L. infantum*; *Lp*, *Leishmania panamensis*; *Ld*, *Leishmania donovani*; *La*, *L. amazonensis*; *Lm*, *Leishmania major*; *Tv*, *Trypanosoma vivax*; *Tb*, *Trypanosoma brucei*; *Tc*, *T. cruzi*; *Tco*, *Trypanosoma congolense*; *Ac*, *Ancylostoma ceylanicum*; *Hs*, *Homo sapiens*; *Bt*, *Bos taurus*; *Pc*, *Pseudosciaena crocea*; *Mm*, *Mus musculus*; *Sm*, *Schistosoma mansoni*; *Pv*, *Plasmodium vivax*; *Sc*, *S. cerevisiae*; *Hp*, *Helicobacter pylori*; *Mt*, *Mycobacterium tuberculosis*; *Se*, *Salmonella enterica*. *b*, 3D alignment of cation-independent 2-Cys Prx showing the highly conserved water that links the Asp/Ser cluster at the A-type interface. Note the high conservation at positions 108 and 109 in contrast with the higher variability at position 112 (facultative role in cation or water coordination) and position 76 (the main chain involved in cation/water binding). PDB accession codes are in *parentheses*.

By converting *Lb*Prx1m into a cation-independent 2-Cys Prx, we have provided strong evidence that the microenvironment of Asp-108 selects *Lb*Prx1m as a Ca^{2+}/Mg^{2+}-sensitive Prx1. According to our model, *Lb*Prx1m requires Ca^{2+}/Mg^{2+} to surpass the electrostatic attraction caused by Lys-137 on Asp-108 and to restore the solvent-mediated link that holds the main chain of Asp-76 and contributes to maintain the fully folded conformation of the C_P-loop, which is mandatory for substrate binding and catalysis. Comparative sequence analysis suggests that the high Ca^{2+}/Mg^{2+} sensitivity observed for *Lb*PRx1m extends exclusively to mitochondrial 2-Cys Prx from the *Leishmania* species (Fig. 12).

Ca^{2+}/Mg^{2+} ions compose a redundant molecular system that supports the chaperone function in vivo

Our studies have demonstrated the similar efficiency of oxidized and reduced cation-stabilized decamers in preventing luciferase aggregation under heat stress conditions. This finding suggests that the *Leishmania* reservoir of Prx1m chaperones is not only formed by reduced proteins, as envisaged previously (3), but can also comprise oxidized Prx1m (S–S-bonded). As the S–S-bonded species represent about half of the Prx1m population present in the parasite (2), their capability to

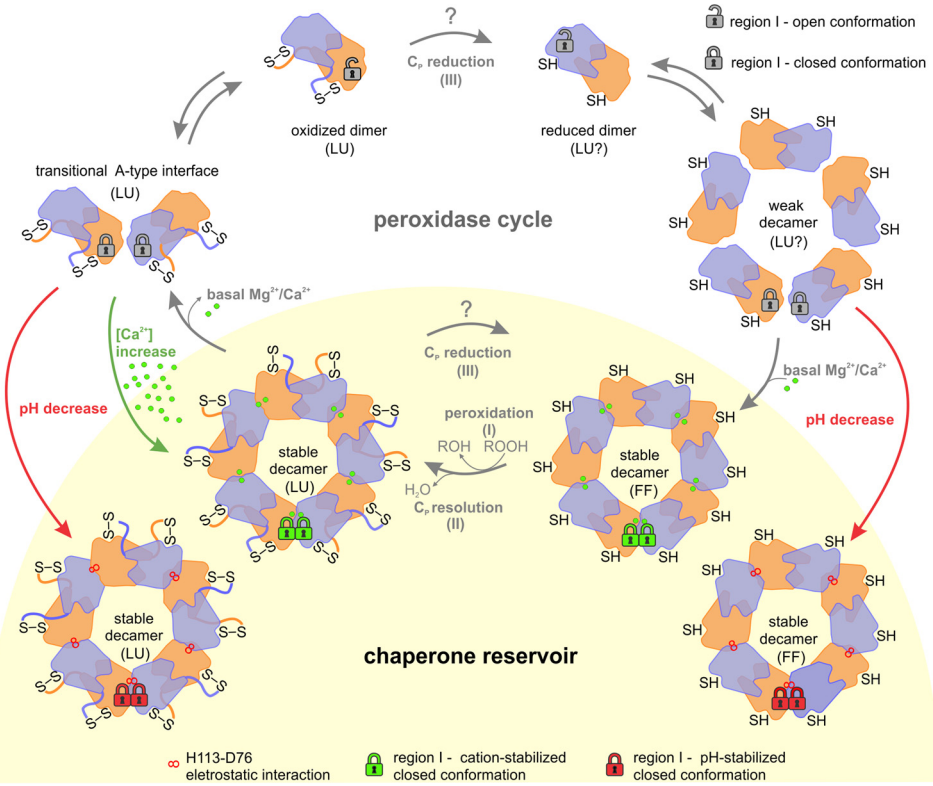

Figure 13. Physiological role of Mg^{2+}/Ca^{2+}, pH, and redox state in the maintenance of the chaperone reservoir of mitochondrial Prx1 in *Leishmania*. During the peroxidase cycle, *Leishmania* Prx1m transits between the dimeric (chaperone-inactive) and the decameric (chaperone-active) forms. This oligomeric shift is regulated by the conformational changes of two regions from the loop-helix active-site motif: the C_p-loop (*LU* ⇔ *FF*), which is redox-sensitive, and the region I (open ⇔ closed), which is Ca^{2+}/Mg^{2+}/pH-sensitive. When dimers are reduced (*SH*), they tend to form weak decamers in which free Mg^{2+} and Ca^{2+} ions bind to enhance their peroxidase and chaperone functions. In basal conditions, after the peroxidation (I) and resolution (II) steps, oxidized (S–S) decamers tend to release Mg^{2+} and Ca^{2+} ions and dissociate into dimers, a process that involves an intermediate state, here named the transitional A-type interface. However, under heat-stress conditions, two stimuli can boost the chaperone reservoir of Prx1m, mainly by stabilizing the oxidized decamers: *red arrows*, small pH decreases; *green arrows*, Ca^{2+} overload. Because our data could not discriminate the preferable substrate for tryparedoxin (Prx1m dimers or decamers), we labeled the C_p reduction step with a *question mark*. The same is applicable for the conformational state proposed for the active site in reduced dimers and reduced weak decamers. For purposes of clarity, the *padlocks* illustrating the conformational state of region I are shown only for a pair of dimers at the decamers. *LU*, locally unfolded; *FF*, fully folded.

form chaperone-active decamers may be of great relevance for *Leishmania* virulence, considering that the chaperone function of Prx1m is crucial for the parasite survival in the mammalian host (3). Moreover, the resistance of *Leishmania* Prx1m to C_p overoxidation (2) and the lack of the sulfiredoxin protein in these parasites further supports the importance of an alternative mechanism to modulate the chaperone activity of Prx1m in *Leishmania* species.

When *Lb*Prx1m dimers fail to respond to the three components of the decamer-stabilizing system (pH, redox state, and Ca^{2+}/Mg^{2+}), they lose their capacity to rescue the temperature-sensitive phenotype of *prx1m*$^{-}$ promastigotes, as indicated by our studies with mutant H113A. Based on our results, we suggest that the residue His-113 is not directly involved in cation binding but is necessary for the formation of a transitional A-type interface that is then stabilized by cation binding, His-113 protonation (9), or less effectively, by C_p reduction. The crystal structure of oxidized *Lb*Prx1m dimers shows that region I preceding the C_p-loop is highly flexible and can transit between an open and a closed conformation, which favors dimers and decamers, respectively (9). The prerequisite to form transitional A-type interfaces likely involves the H-bond between His-113 and Asp-76 when region I accesses the closed conformation. Because this interaction is insufficient to lock region I in the closed conformation, decamer stabilization requires a second stimulus.

According to our model (Fig. 13), in basal concentrations of enzyme, Mg^{2+}, and Ca^{2+}, most of Prx1m enzymes are decameric when reduced and dimeric when oxidized. During heat shock, which stimulates Ca^{2+} uptake in *Leishmania* promastigotes (34), higher levels of Ca^{2+} at the mitochondrion (27) feed the chaperone reservoir with oxidized decamers. Besides stimulating mitochondrial Ca^{2+} uptake, cytosolic Ca^{2+} elevations can also lead to a mitochondrial pH decrease of about 0.2 pH units (35), providing an extra stimulus to enlarge the reservoir of Prx1m decamers (9). At pH 7, for example, we detected *in vitro* a cooperative effect between pH and Ca^{2+} in stabilizing oxidized decamers (data not shown).

Together, our studies show that basal concentrations of Mg^{2+}/Ca^{2+} ions support the dual function of mitochondrial Prx1 from *Leishmania* and reveal a molecular mechanism that may help explain why calcium uptake is crucial for *Leshimania* thermotolerance and differentiation in the mammalian host (34). Furthermore, we have demonstrated that the decameric structure, independently of its redox state, is both necessary and sufficient for the protective effect of Prx1m against heat

stress in *Leishmania*, a vital attribute for the establishment of a successful infection in the mammalian host (2, 3). This finding implies that the search for compounds that prevent Prx1m decamerization represents the best strategy for inhibiting the crucial chaperone function of this attractive therapeutic target (36). Zhao *et al.* (37) already have identified chaperone inhibitors for the human Prx I, demonstrating the feasibility of such an approach.

Experimental procedures

Molecular cloning and site-directed mutagenesis

The *Lb*Prx1m gene (RefSeq accession no. XM_001562186.1) was cloned into a pET28a-His-TEV vector as described previously (38). Human gene *PRX2* (RefSeq accession no. NM_005809.5) was amplified by PCR and cloned into the pET28a vector between the NdeI and SalI restriction sites. The *TSA1* gene from *Saccharomyces cerevisiae* was cloned into the pET15b vector as described previously (39). The pET28a construct containing the DNA sequence of the *Lb*Prx1a gene (RefSeq accession no. XM_001563506.1) between the NdeI and SalI restriction sites was purchased from GenScript (Piscataway, NJ). All *Lb*Prx1m mutants were produced using the QuikChange™ site-directed mutagenesis kit (Stratagene).

Protein expression and purification

The protein *Lb*Prx1m and corresponding muteins were expressed and purified as described previously (9). *Lb*Prx1a and *Hs*Prx2 were produced in *E. coli* BL21(DE3)Δ*SlyD* cells containing the plasmid pRARE2, whereas *TSA1* was produced in BL21(DE3) cells. After the cell culture reached $A_{600\ nm} \sim 0.6$ in LB medium, protein expression was induced with 0.5 mM isopropyl 1-thio-β-D-galactopyranoside at 30 °C for 4 h at 200 rpm (*Hs*Prx2 and *Lb*Prx1a) or with 1 mM isopropyl 1-thio-β-D-galactopyranoside at 37 °C for 3 h at 200 rpm (*TSA1*). Protein extraction and affinity purification followed that described for *Lb*Prx1m (9). All purified proteins were dialyzed against the buffer used in the analytical size-exclusion chromatography step and concentrated using Amicon Ultra devices (Millipore). The oxidized (S–S-bonded) state of the purified proteins was confirmed by SDS-PAGE analysis under non-reducing conditions, whereas the reduced state of proteins treated with DTT was confirmed by quantification of free thiol groups using 5,5′-dithiobis(nitrobenzoic acid) as described previously (9).

Analytical size-exclusion chromatography

A total of 2 ml of *Lb*Prx1m at 130 μM, *Lb*Prx1a at 43 μM, yeast *TSA1* at 43 μM, and *Hs*Prx2 at 130 μM were loaded onto a HiLoad 16/600 Superdex 200 column (GE Healthcare) pre-equilibrated with 25 mM Tris-HCl (pH 7.5) containing 25 mM $CaCl_2$, 25 mM $MgCl_2$, 5 mM EDTA, or 5 mM EGTA. aSEC experiments for the *Lb*Prx1m mutants D108A, S109A, and S112A at 86 μM (500 μl input) were carried out using the same column pre-equilibrated with buffer T-Ca (25 mM Tris-HCl, 150 mM NaCl, and 25 mM $CaCl_2$, pH 7.5). The same assay was performed using the mutant C107M/M139K at 86 μM (500 μl input) in buffer T-EDTA (25 mM Tris-HCl, 150 mM NaCl, and 5 mM EDTA, pH 7.5). Additionally, WT *Lb*Prx1m was cleaved with TEV protease to remove the His tag, preincubated at 94 μM with or without 10 mM DTT in buffer T-Ca or T-EDTA, and divided into three samples at different protein concentrations (94, 23, and 9 μM) that were loaded (250 μl) onto a Superdex 200 10/300 GL column (GE Healthcare) pre-equilibrated with the sample buffer.

aSEC assays mimicking *in vivo* conditions (3, 25–27, 40, 41) were performed with TEV-cleaved *Lb*Prx1m at 100 μM (200 μl input) in buffer T-EDTA plus the following additives: 5.7 mM $MgCl_2$ (free $Mg^{2+} = 0.7$ mM) and 200 nM $CaCl_2$ (condition I); and the same as described in condition I but with 90 μM $CaCl_2$ (condition II). These assays were carried out in a Superdex 200 10/300 GL column (GE Healthcare). Samples were pretreated and eluted in the presence of 2 mM DTT or pretreated with 2 mM DTT, re-oxidized, and eluted in buffer without DTT. To obtain re-oxidized samples, DTT was removed as described by Morais *et al.* (9), and the concentrated protein was incubated with H_2O_2 in a 1:1 (protein:H_2O_2) molar ratio prior injection. The redox state of the samples was analyzed by non-reducing SDS-PAGE.

aSEC assays of *Lb*Prx1m WT and S112A mutant at 13 μM (200 μl input) were performed in buffer T-Ca using a Superdex 200 10/300 GL column (GE Healthcare). Additional aSEC assays comparing WT *Lb*Prx1m and H113A and D108A mutants at 48 μM (250 μl input) were performed at pH 4.0, as described in Morais *et al.* (9), in buffer T-EDTA plus 2 mM DTT or in buffer T-Ca. For comparative purposes, the molar concentrations estimated for all analyzed proteins refer to monomers. Columns were calibrated using the gel filtration calibration kits LMW and HMW (GE Healthcare).

Dynamic light scattering (DLS)

DLS measurements were performed on a Dynapro molecular sizing instrument at 25 or 42 °C. Protein samples at 100 μM were centrifuged previously for 20 min at 20,000 × *g*. Data were collected at intervals of 10 s with at least 100 acquisitions. The diffusion coefficient (*D*) was determined from the analysis of measured time-dependent fluctuations in the scattering intensity and used to calculate the hydrodynamic radius (R_H) of the protein according to the Stokes-Einstein equation. Data analysis was performed using the software Dynamics V6.3.40.

Small angle X-ray scattering

SAXS data were collected at the D02A/SAXS2 beamline (Brazilian Synchrotron Light Laboratory, Campinas, Brazil). The radiation wavelength was set to 1.48 Å and a 165-mm MarCCD detector was used to record the scattering patterns. The sample-to-detector distance was set to 1534.5 mm to give a scattering vector range from 0.25 to 2.5 nm^{-1}. Protein samples at 108 μM were prepared in 25 mM Tris-HCl (pH 7.5) with 5 mM EDTA or 25 mM $CaCl_2$. Frames with an exposure time of 600 s were recorded, and buffer baselines were collected under identical conditions. Background scattering was subtracted from the protein-scattering pattern, which was then normalized and corrected. Experimental data fitting and evaluation of the pair-distance distribution function *P*(r) were performed using the program GNOM (42). The low-resolution envelopes were determined using *ab initio* modeling as implemented in the

program DAMMIN (43). An averaged model was generated using the package DAMAVER (44) The low-resolution model and the crystal structure were superimposed using the program SUPCOMB (45).

Fluorescence anisotropy measurements

Fluorescence anisotropy data were collected in a PC-1 fluorimeter (ISS Instruments) coupled to a thermal bath at 25 °C using an excitation wavelength of 280 nm (46). Samples of *Lb*Prx1m at 80 μM were preincubated in buffer at pH 7.5 containing 25 mM Tris-HCl, 150 mM NaCl, and 5 mM EDTA and increasing amounts of $CaCl_2$ or $MgCl_2$. For data acquisition, samples were diluted in buffer consisting of 25 mM Tris-HCl and 150 mM NaCl (pH 7.5) to a final protein concentration of 2 μM. Free cation concentrations were defined by subtracting the added $Ca(Mg)Cl_2$ concentration from the EDTA concentration of each sample. The mean data of three independent experiments were fitted to a nonlinear regression to estimate the constant $K_{½}$ using GraphPad Prism v.6.0.

Molecular dynamics simulations

The most favorable geometric coordination of Ca^{2+} by the residues Ser-109$^{(chain\ A)}$, Ser-112$^{(chain\ A)}$, Asp-76$^{(chain\ J)}$ and Asp-108$^{(chain\ J)}$ of the *Lb*Prx1m decamer (PDB accession no. 4KB3) was evaluated using molecular dynamics simulations. The system was submitted to an explicit solvent simulation with a water density of 1 g cm^{-3} and neutralized using a 0.9% NaCl solvent (mass fraction) at 298 K. The protonation states for ionizable groups were set according to pH 7.0 using an empirical equation derived from experimental data that considers electrostatic potential, hydrogen bonds, and accessible surface area (47). The simulation was carried out for 10 ns using the YAMBER3 force field (48), which includes the cation parameters, on the program YASARA. The calcium coordination sphere for every 25-ps snapshot was analyzed using a customized script implemented in FindGeo (49).

Enzymatic assays

NADPH consumption (ε340 nm = 6220 M^{-1} cm^{-1}) by the *Leishmania* trypanothione system was monitored at 340 nm in a Shimatzu UV-2401 spectrophotometer (Shimatzu Corp.) with temperature set to 25 °C. The reactions were carried out with 280 μM NADPH, 0.4 μM trypanothione reductase *LiTR* (50), 75 μM trypanothione (Bachem), 4 μM tryparedoxin *Li*TXN1 (50), and 4.5 μM *Lb*Prx1m (WT or mutants) or 0.4 μM *Li*Prx1a (50) in a buffer consisting of 50 mM Tris-HCl (pH 7.5). *Li*TR and trypanothione were used in excess. The Prx enzyme was either untreated or pretreated with 5 mM EDTA or 5 mM EDTA followed by the addition of 25 mM $CaCl_2$ or $MgCl_2$. The others components were incubated previously at 25 °C for 15 min. The treated Prx samples were diluted in the reaction medium, and the reaction was started with the addition of 70 μM H_2O_2. All experiments were performed with TEV-cleaved *Lb*Prx1m in triplicate. Relative activities were calculated as mean values considering the untreated samples as a reference for the cation and EDTA treatments or the WT activity of *Lb*Prx1m in the presence of $CaCl_2$ as a reference for the muteins assayed under the same conditions.

Chaperone activity assays

To investigate the chaperone activity of reduced and oxidized *Lb*Prx1m (WT or mutants), 100 nM luciferase (Promega) was incubated in 40 mM HEPES (pH 7.5) at 42 °C with a molar ratio of 1:10 (Luciferase:*Lb*Prx1m). *Lb*Prx1m was pretreated with 20 mM $CaCl_2$ or $MgCl_2$, 5 mM EDTA, or 5 mM EDTA plus 25 mM $CaCl_2$ or $MgCl_2$. The reduced samples were incubated with 2 mM DTT (final concentration). The reactions were kept at 42 °C, and luciferase aggregation was monitored in a Fluoromax-4 spectrofluorometer (Horiba) for 900 s using a wavelength of 360 nm for excitation and emission. Relative activities were calculated as mean values considering the activity of untreated samples as reference for those treated with additives (Ca^{2+}, EDTA, and DTT) or the activity of WT protein as a reference for the muteins assayed in the same condition, unless stated otherwise. To exclude the effect that some additives have on luciferase aggregation, the relative activities were calculated according to the formula $(N_T - T)/(N_R - R)$, where N_T, T, N_R, and R refer to light-scattering values recorded at 900 s of N_T, the negative control reaction of the test condition (luciferase + additives); T is the test condition (N_T + WT or mutant *Lb*Prx1m); N_R is the negative control reaction of the reference condition (luciferase + additives); and R is the reference condition (N_R+ WT *Lb*Prx1m). All assays were performed with TEV-cleaved *Lb*Prx1m in triplicate.

Circular dichroism

CD measurements were acquired at 25 or 42 °C on a JASCO J-815 spectropolarimeter equipped with a Peltier temperature controller (Jasco Analytical Instruments). TEV-cleaved *Lb*Prx1m samples (WT and H113A mutant) at 80 μM were pretreated with 5 mM EDTA plus (or not) 25 mM $CaCl_2$ and diluted to a final concentration of 2 μM in 10 mM sodium phosphate (pH 7.5) with or without 2 mM DTT. Far-UV CD spectra were recorded between 190 and 260 nm at a speed of 50 nm/min with a total of 16 accumulations. The CD data were buffer-subtracted and normalized to molar residual ellipticity allowing the comparison between different treatments.

Differential scanning fluorimetry

DSF assays were performed in triplicate using a real-time PCR machine 7300 (Applied Biosystems). Samples of TEV-cleaved *Lb*Prx1m (WT and H113A mutant) were pretreated as described above and diluted to a final concentration of 2 μM in buffer consisting of 20 mM HEPES (pH 7.5), 150 mM NaCl, with or without 2 mM DTT, and containing 5× SYPRO Orange fluorescent dye (Invitrogen-Molecular Probes). The 96-well plates were heated from 25 to 95 °C, increasing 1 °C/cycle, and the fluorescence emission was measured at 580 nm. The DSF melting curves were analyzed using GraphPad Prism software version 6.0.

Generation of L. infantum transfectants

To construct the pSSU-PHLEO-infantum-*Lb*Prx1m plasmids, a DNA fragment corresponding to the mitochondrial targeting sequence of Prx1m was PCR-amplified with *Pfu*Turbo from genomic DNA of *Leishmania amazonensis* with primers

P1 (5′-cgc*ggatcc*ATGCTCCGTCGTCTTGCTA-3′) and P2 (5′-tgc*tctagagctagcaggcct*GACAGTCGCCGTACGGTA-3′) and cloned into the BamHI and XbaI sites of pSSU-PHLEO-infantum-*Li*Prx1m vector (2). Clamp sequences are indicated in lower case, and restriction sites are in italics. The resulting plasmid was subsequently digested with StuI and NheI and ligated to the rest of the *Lb*Prx1m ORF (either the WT or mutated versions of the gene) obtained by PCR amplification with *Pfu*-Turbo and primers P3 (5′-GATCCTGCGCCGCAGTTT-3′) and P4 (5′-cta*gctagc*TCACATATTCTTCTCAAAAAATT-3′) from the plasmids pET28a-His-TEV-*Lb*Prx1m WT or mutants. The accuracy of all constructs was verified by DNA sequencing at GATC Biotech (Konstanz, Germany). Prior to transfection of *L. infantum*, the pSSU-PHLEO-infantum-*Lb*Prx1m constructs were linearized by digestion with NdeI and PmeI and purified from agarose gels.

Transfection of L. infantum and isolation of mutants

Transfections were carried out on *L. infantum* promastigotes (MHOM MA67ITMAP263) missing both Prx1m alleles (*i.e.* Prx1m null mutants or *Prx1m*$^{-}$) produced previously (2). Parasites were grown to the logarithmic phase and electroporated at 450 V and 350–400 μF with 5 μg of DNA as described elsewhere (51). Transfectants were allowed to recover in culture medium without selective drug for 24 h prior to being plated onto agar plates containing 17.5 μg ml^{-1} bleomycin (Sigma-Aldrich). Upon 1 to 2 weeks of growth on agar, colonies were picked up, transferred to liquid medium, and analyzed by PCR, Western blotting, and indirect immunofluorescence to confirm *Lb*Prx1m expression in the transfectants according to previously described procedures (2, 52).

Thermotolerance assays

L. infantum promastigotes, synchronized previously by three to four daily changes of culture medium, were seeded at 10^6 cells ml^{-1} in 24-well plates containing RPMI 1640-GlutaMAX medium supplemented with 10% inactivated fetal bovine serum, 50 units ml^{-1} penicillin, 50 mg ml^{-1} streptomycin (all from Gibco), and 20 mM HEPES sodium salt (pH 7.4) (Sigma). Parasites were allowed to grow for 4 days at either 25 or 37 °C. Every 24 h, cell densities were determined with a Neubauer counting chamber for growth curve determination. Two independent clones were analyzed for each transfectant.

Author contributions—M. A. B. M., P. O. G., T. A. C. B. S., H. C., R. V. H., P. S. L. O., L. E. S. N., A. M. T., and M. T. M. conceived and designed the experiments. M. A. B. M., P. O. G., T. A. C. B. S., H. C., and R. V. H. performed the experiments. M. A. B. M., P. O. G., T. A. C. B. S., H. C., R. V. H., P. S. L. O., L. E. S. N., A. M. T., and M. T. M. analyzed the data. M. A. B. M., P. O. G., and M. T. M. wrote the paper, and M. A. B. M., P. O. G., T. A. C. B. S., H. C., R. V. H., P. S. L. O., L. E. S. N., A. M. T., and M. T. M. revised the paper.

Acknowledgments—We are grateful to the Brazilian Synchrotron Light Laboratory (LNLS) and Brazilian Biosciences National Laboratory (LNBio) for the provision of time on MX2 and SAXS1 beamlines, ROBOLAB, LPP, and LEC.

References

1. Pearson, R. D., and Wilson, M. E. (1989) Host defenses against prototypical intracellular protozoans, the *Leishamania*, in *Parasitic Infections in the Compromised Host* (Walzer, P. D., and Genta, R. M., eds) pp 31–81, Marcel Dekker, New York
2. Castro, H., Teixeira, F., Romao, S., Santos, M., Cruz, T., Flórido, M., Appelberg, R., Oliveira, P., Ferreira-da-Silva, F., and Tomás, A. M. (2011) *Leishmania* mitochondrial peroxiredoxin plays a crucial peroxidase-unrelated role during infection: insight into its novel chaperone activity. *PLoS Pathog.* **7,** e1002325
3. Teixeira, F., Castro, H., Cruz, T., Tse, E., Koldewey, P., Southworth, D. R., Tomás, A. M., and Jakob, U. (2015) Mitochondrial peroxiredoxin functions as crucial chaperone reservoir in *Leishmania infantum*. *Proc. Natl. Acad. Sci. U.S.A.* **112,** E616–E624
4. Wood, Z. A., Schröder, E., Robin Harris, J., and Poole, L. B. (2003) Structure, mechanism and regulation of peroxiredoxins. *Trends Biochem. Sci.* **28,** 32–40
5. Jang, H. H., Lee, K. O., Chi, Y. H., Jung, B. G., Park, S. K., Park, J. H., Lee, J. R., Lee, S. S., Moon, J. C., Yun, J. W., Choi, Y. O., Kim, W. Y., Kang, J. S., Cheong, G. W., Yun, *et al.* (2004) Two enzymes in one: two yeast peroxiredoxins display oxidative stress-dependent switching from a peroxidase to a molecular chaperone function. *Cell* **117,** 625–635
6. Moon, J. C., Hah, Y. S., Kim, W. Y., Jung, B. G., Jang, H. H., Lee, J. R., Kim, S. Y., Lee, Y. M., Jeon, M. G., Kim, C. W., Cho, M. J., and Lee, S. Y. (2005) Oxidative stress-dependent structural and functional switching of a human 2-Cys peroxiredoxin isotype II that enhances HeLa cell resistance to H2O2-induced cell death. *J. Biol. Chem.* **280,** 28775–28784
7. Chuang, M. H., Wu, M. S., Lo, W. L., Lin, J. T., Wong, C. H., and Chiou, S. H. (2006) The antioxidant protein alkylhydroperoxide reductase of *Helicobacter pylori* switches from a peroxide reductase to a molecular chaperone function. *Proc. Natl. Acad. Sci. U.S.A.* **103,** 2552–2557
8. Bernier-Villamor, L., Navarro, E., Sevilla, F., and Lázaro, J. J. (2004) Cloning and characterization of a 2-Cys peroxiredoxin from *Pisum sativum*. *J. Exp. Bot.* **55,** 2191–2199
9. Morais, M. A., Giuseppe, P. O., Souza, T. A., Alegria, T. G., Oliveira, M. A., Netto, L. E., and Murakami, M. T. (2015) How pH modulates the dimer-decamer interconversion of 2-Cys peroxiredoxins from the Prx1 subfamily. *J. Biol. Chem.* **290,** 8582–8590
10. Kristensen, P., Rasmussen, D. E., and Kristensen, B. I. (1999) Properties of thiol-specific anti-oxidant protein or calpromotin in solution. *Biochem. Biophys. Res. Commun.* **262,** 127–131
11. Kitano, K., Niimura, Y., Nishiyama, Y., and Miki, K. (1999) Stimulation of peroxidase activity by decamerization related to ionic strength: AhpC protein from *Amphibacillus xylanus*. *J. Biochem.* **126,** 313–319
12. Matsumura, T., Okamoto, K., Iwahara, S., Hori, H., Takahashi, Y., Nishino, T., and Abe, Y. (2008) Dimer-oligomer interconversion of wild-type and mutant rat 2-Cys peroxiredoxin: disulfide formation at dimer-dimer interfaces is not essential for decamerization. *J. Biol. Chem.* **283,** 284–293
13. Barranco-Medina, S., Kakorin, S., Lázaro, J. J., and Dietz, K. J. (2008) Thermodynamics of the dimer-decamer transition of reduced human and plant 2-Cys peroxiredoxin. *Biochemistry* **47,** 7196–7204
14. Guimarães, B. G., Souchon, H., Honoré, N., Saint-Joanis, B., Brosch, R., Shepard, W., Cole, S. T., and Alzari, P. M. (2005) Structure and mechanism of the alkyl hydroperoxidase AhpC, a key element of the *Mycobacterium tuberculosis* defense system against oxidative stress. *J. Biol. Chem.* **280,** 25735–25742
15. Wood, Z. A., Poole, L. B., Hantgan, R. R., and Karplus, P. A. (2002) Dimers to doughnuts: redox-sensitive oligomerization of 2-cysteine peroxiredoxins. *Biochemistry* **41,** 5493–5504
16. Wood, Z. A., Poole, L. B., and Karplus, P. A. (2003) Peroxiredoxin evolution and the regulation of hydrogen peroxide signaling. *Science* **300,** 650–653
17. Sarkar, A. R., Heo, C. H., Xu, L., Lee, H. W., Si, H. Y., Byun, J. W., and Kim, H. M. (2016) A ratiometric two-photon probe for quantitative imaging of mitochondrial pH values. *Chem. Sci.* **7,** 766–773

18. Chauhan, R., and Mande, S. C. (2001) Characterization of the *Mycobacterium tuberculosis* H37Rv alkyl hydroperoxidase AhpC points to the importance of ionic interactions in oligomerization and activity. *Biochem. J.* **354,** 209–215
19. Park, J. W., Piszczek, G., Rhee, S. G., and Chock, P. B. (2011) Glutathionylation of peroxiredoxin I induces decamer to dimers dissociation with concomitant loss of chaperone activity. *Biochemistry* **50,** 3204–3210
20. Engelman, R., Weisman-Shomer, P., Ziv, T., Xu, J., Arnér, E. S., and Benhar, M. (2013) Multilevel regulation of 2-Cys peroxiredoxin reaction cycle by *S*-nitrosylation. *J. Biol. Chem.* **288,** 11312–11324
21. Bui, D. M., Gregan, J., Jarosch, E., Ragnini, A., and Schweyen, R. J. (1999) The bacterial magnesium transporter CorA can functionally substitute for its putative homologue Mrs2p in the yeast inner mitochondrial membrane. *J. Biol. Chem.* **274,** 20438–20443
22. McCormack, J. G., Halestrap, A. P., and Denton, R. M. (1990) Role of calcium ions in regulation of mammalian intramitochondrial metabolism. *Physiol. Rev.* **70,** 391–425
23. Huang, G., Vercesi, A. E., and Docampo, R. (2013) Essential regulation of cell bioenergetics in *Trypanosoma brucei* by the mitochondrial calcium uniporter. *Nat. Commun.* **4,** 2865
24. Tsien, R. Y. (1980) New calcium indicators and buffers with high selectivity against magnesium and protons: design, synthesis, and properties of prototype structures. *Biochemistry* **19,** 2396–2404
25. Kolisek, M., Zsurka, G., Samaj, J., Weghuber, J., Schweyen, R. J., and Schweigel, M. (2003) Mrs2p is an essential component of the major electrophoretic Mg2+ influx system in mitochondria. *EMBO J.* **22,** 1235–1244
26. Rutter, G. A., Burnett, P., Rizzuto, R., Brini, M., Murgia, M., Pozzan, T., Tavaré, J. M., and Denton, R. M. (1996) Subcellular imaging of intramitochondrial Ca2+ with recombinant targeted aequorin: significance for the regulation of pyruvate dehydrogenase activity. *Proc. Natl. Acad. Sci. U.S.A.* **93,** 5489–5494
27. Benaim, G., Bermudez, R., and Urbina, J. A. (1990) Ca2+ transport in isolated mitochondrial vesicles from *Leishmania braziliensis* promastigotes. *Mol. Biochem. Parasitol.* **39,** 61–68
28. Simonovic, M., Dolmer, K., Huang, W., Strickland, D. K., Volz, K., and Gettins, P. G. (2001) Calcium coordination and pH dependence of the calcium affinity of ligand-binding repeat CR7 from the LRP: comparison with related domains from the LRP and the LDL receptor. *Biochemistry* **40,** 15127–15134
29. Suzuki, N., Fujimoto, Z., Morita, T., Fukamizu, A., and Mizuno, H. (2005) pH-Dependent structural changes at Ca(2+)-binding sites of coagulation factor IX-binding protein. *J. Mol. Biol.* **353,** 80–87
30. Nelson, K. J., Knutson, S. T., Soito, L., Klomsiri, C., Poole, L. B., and Fetrow, J. S. (2011) Analysis of the peroxiredoxin family: using active-site structure and sequence information for global classification and residue analysis. *Proteins* **79,** 947–964
31. Piñeyro, M. D., Pizarro, J. C., Lema, F., Pritsch, O., Cayota, A., Bentley, G. A., and Robello, C. (2005) Crystal structure of the tryparedoxin peroxidase from the human parasite *Trypanosoma cruzi*. *J. Struct. Biol.* **150,** 11–22
32. Parsonage, D., Youngblood, D. S., Sarma, G. N., Wood, Z. A., Karplus, P. A., and Poole, L. B. (2005) Analysis of the link between enzymatic activity and oligomeric state in AhpC, a bacterial peroxiredoxin. *Biochemistry* **44,** 10583–10592
33. Casey, J. R., Grinstein, S., and Orlowski, J. (2010) Sensors and regulators of intracellular pH. *Nat. Rev. Mol. Cell Biol.* **11,** 50–61
34. Prasad, A., Kaur, S., Malla, N., Ganguly, N. K., and Mahajan, R. C. (2001) Ca2+ signaling in the transformation of promastigotes to axenic amastigotes of *Leishmania donovani*. *Mol. Cell. Biochem.* **224,** 39–44
35. Poburko, D., Santo-Domingo, J., and Demaurex, N. (2011) Dynamic regulation of the mitochondrial proton gradient during cytosolic calcium elevations. *J. Biol. Chem.* **286,** 11672–11684
36. Angelucci, F., Miele, A. E., Ardini, M., Boumis, G., Saccoccia, F., and Bellelli, A. (2016) Typical 2-Cys peroxiredoxins in human parasites: several physiological roles for a potential chemotherapy target. *Mol. Biochem. Parasitol.* **206,** 2–12
37. Zhao, Q., Ding, Y., Deng, Z., Lee, O. Y., Gao, P., Chen, P., Rose, R. J., Zhao, H., Zhang, Z., Tao, X. P., Heck, A. J., Kao, R., and Yang, D. (2015) Natural products triptolide, celastrol, and withaferin A inhibit the chaperone activity of peroxiredoxin I. *Chem. Sci.* **6,** 4124–4130
38. de Morais, M. A., de Souza, Tde A., and Murakami, M. T. (2013) Cloning, expression, purification, crystallization and preliminary X-ray diffraction analysis of the mitochondrial tryparedoxin peroxidase from *Leishmania braziliensis*. *Acta Crystallogr. Sect. F Struct. Biol. Cryst. Commun.* **69,** 408–411
39. de Oliveira, M. A., Genu, V., Discola, K. F., Alves, S. V., Netto, L. E., and Guimarães, B. G. (2007) Crystallization and preliminary X-ray analysis of a decameric form of cytosolic thioredoxin peroxidase 1 (Tsa1), C47S mutant, from *Saccharomyces cerevisiae*. *Acta Crystallogr. Sect. F Struct. Biol. Cryst. Commun.* **63,** 665–668
40. Rutter, G. A., Osbaldeston, N. J., McCormack, J. G., and Denton, R. M. (1990) Measurement of matrix-free Mg2+ concentration in rat heart mitochondria by using entrapped fluorescent probes. *Biochem. J.* **271,** 627–634
41. Montero, M., Alonso, M. T., Carnicero, E., Cuchillo-Ibáñez, I., Albillos, A., García, A. G., García-Sancho, J., and Alvarez, J. (2000) Chromaffin-cell stimulation triggers fast millimolar mitochondrial Ca2+ transients that modulate secretion. *Nat. Cell Biol.* **2,** 57–61
42. Svergun, D. (1992) Determination of the regularization parameter in indirect-transform methods using perceptual criteria. *J. Appl. Crystallogr.* **25,** 495–503
43. Svergun, D. I. (1999) Restoring low resolution structure of biological macromolecules from solution scattering using simulated annealing. *Biophys. J.* **76,** 2879–2886
44. Volkov, V., and Svergun, D. (2003) Uniqueness of *ab initio* shape determination in small-angle scattering. *J. Appl. Crystallogr.* **36,** 860–864
45. Kozin, M. B., and Svergun, D. I. (2001) Automated matching of high- and low-resolution structural models. *J. Appl. Crystallogr.* **34,** 33–41
46. LeTilly, V., and Royer, C. A. (1993) Fluorescence anisotropy assays implicate protein-protein interactions in regulating trp repressor DNA binding. *Biochemistry* **32,** 7753–7758
47. Krieger, E., Nielsen, J. E., Spronk, C. A., and Vriend, G. (2006) Fast empirical pKa prediction by Ewald summation. *J. Mol. Graph. Model.* **25,** 481–486
48. Krieger, E., Darden, T., Nabuurs, S. B., Finkelstein, A., and Vriend, G. (2004) Making optimal use of empirical energy functions: force-field parameterization in crystal space. *Proteins* **57,** 678–683
49. Andreini, C., Cavallaro, G., and Lorenzini, S. (2012) FindGeo: a tool for determining metal coordination geometry. *Bioinformatics* **28,** 1658–1660
50. Castro, H., Sousa, C., Novais, M., Santos, M., Budde, H., Cordeiro-da-Silva, A., Flohé, L., and Tomás, A. M. (2004) Two linked genes of *Leishmania infantum* encode tryparedoxins localised to cytosol and mitochondrion. *Mol. Biochem. Parasitol.* **136,** 137–147
51. Beverley, S. M., and Clayton, C. E. (1993) Transfection of *Leishmania* and *Trypanosoma brucei* by electroporation. *Methods Mol. Biol.* **21,** 333–348
52. Sousa, A. F., Gomes-Alves, A. G., Benítez, D., Comini, M. A., Flohé, L., Jaeger, T., Passos, J., Stuhlmann, F., Tomás, A. M., and Castro, H. (2014) Genetic and chemical analyses reveal that trypanothione synthetase but not glutathionylspermidine synthetase is essential for *Leishmania infantum*. *Free Radic. Biol. Med.* **73,** 229–238
53. Castro, H., Sousa, C., Santos, M., Cordeiro-da-Silva, A., Flohé, L., and Tomás, A. M. (2002) Complementary antioxidant defense by cytoplasmic and mitochondrial peroxiredoxins in *Leishmania infantum*. *Free Radic. Biol. Med.* **33,** 1552–1562